Interannual variations in the $\Delta'(^{17}O)$ signature of atmospheric CO_2 at two mid-latitude sites suggest a close link to stratosphere-troposphere exchange

Pharahilda M. Steur[1], Hubertus A. Scheeren[1], Gerbrand Koren[2], Getachew A. Adnew[3*], Wouter Peters[1,4], and Harro A. J. Meijer[1]

[1]Centre for Isotope Research (CIO), Energy and Sustainability Research Institute Groningen, University of Groningen, Groningen, the Netherlands
[2]Copernicus Institute of Sustainable Development, Utrecht University, Utrecht, the Netherlands
[3]Institute for Marine and Atmospheric research Utrecht (IMAU), Utrecht University, the Netherlands
[4]Environmental Sciences Group, Dept of Meteorology and Air Quality, Wageningen University and Research, Wageningen, the Netherlands
[*]now at the Department of Geosciences and Natural Resource Management, University of Copenhagen, Copenhagen, Denmark

Correspondence: Pharahilda M. Steur (p.m.steur@rug.nl)

Abstract. $\Delta'(^{17}O)$ measurements of atmospheric CO_2 have the potential to be a tracer for gross primary production and stratosphere-troposphere mixing. A positive $\Delta'(^{17}O)$ originates from intrusions of stratospheric CO_2, whereas values close to -0.21 ‰ result from equilibration of CO_2 and water, predominantly happening inside plants. The stratospheric source of CO_2 carrying high $\Delta'(^{17}O)$ is, however, not well defined in the current models. More and long-time atmospheric measurements are

5 needed to improve this. We present records of the $\Delta'(^{17}O)$ of atmospheric CO_2 conducted with laser absorption spectroscopy, from Lutjewad in the Netherlands (53° 24'N, 6° 21'E) and Mace Head in Ireland (53° 20' N, 9° 54' W), covering the period 2017-2022. The records are compared with a 3-D model simulation, and we study potential model improvements. Both records show significant interannual variability, of up to 0.3 ‰. The total range covered by smoothed monthly averages from the Lutjewad record is -0.34 to -0.12 ‰, which is significantly higher than the range of -0.20 and -0.17 ‰ of the model simulation.

10 The 100 hPa 60-90° North monthly mean temperature anomaly was used as a proxy to scale stratospheric downwelling in the model. This strongly improves the correlation coefficient of the simulated and observed year-to-year $\Delta'(^{17}O)$ variations over the period 2019-2021, from 0.40 to 0.82. As the $\Delta'(^{17}O)$ of atmospheric CO_2 seems to be dominated by stratospheric influx, its use a as a tracer for stratosphere-troposphere exchange should be further investigated.

1 Introduction

15 Stable isotope measurements of atmospheric CO_2 have been a great asset to carbon cycle research (Mook et al., 1983; Keeling et al., 1984; Ciais et al., 1997; Welp et al., 2011; Carlstad and Boering, 2023). As different isotopologues of CO_2 have the same chemical properties and will be incorporated in the same carbon cycle fluxes, their difference in mass can result in preferred uptake or emission of the lighter or heavier isotopologues for certain processes. This is known as kinetic fractionation

(Young et al., 2002). Another form of fractionation is equilibrium fractionation, in which isotopes in different substances at
20   chemical equilibrium are partially separated (Young et al., 2002). Fractionation will thus influence the isotope composition
of atmospheric CO_2, and together with CO_2 amount fraction measurements, the isotope composition of atmospheric CO_2 can
help to disentangle carbon sources and sinks (Peters et al., 2018; Welp et al., 2011; Hofmann et al., 2017; Keeling et al., 2005;
Laskar et al., 2016). Isotope composition is generally expressed relative to an internationally recognised reference material
using the delta notation, according to equation 1:

$$\delta(^*A) = \frac{[^*A_{\mathrm{s}}]/[A_{\mathrm{s}}]}{[^*A_{\mathrm{r}}]/[A_{\mathrm{r}}]} - 1 \tag{1}$$

In which A is the atom (for CO_2 this is C or O), the superscript * stands for the rare isotope (13 for C, 17 or 18 for O), A
without * stands for the most abundant isotope (12 for C, 16 for O) and the subscripts s and r stand for sample and reference,
respectively. Delta values are usually expressed in per mille, indicated by the ‰ symbol, as the natural variation is very small.
Applications of $\delta(^{13}C)$ and $\delta(^{18}O)$ measurements of atmospheric CO_2 are numerous and have proven to be of great value for
30   identification and quantification of sources and sinks of atmospheric CO_2 (Roeloffzen et al., 1991; Ciais et al., 1995; Rayner
et al., 2008) and for the description of air mixing dynamics of the troposphere and stratosphere (Assonov et al., 2010).

     The relation between $\delta(^{17}O)$ and $\delta(^{18}O)$, resulting from the kinetic and equilibrium fractionation processes as described
above is relatively constant and can be described by:

$$\ln(\delta(^{17}O) + 1) = \theta \ln(\delta(^{18}O) + 1) \tag{2}$$

35   With θ ranging between 0.5 and 0.53, depending on the dominant fractionation process studied (Adnew et al., 2022).
From the $\delta(^{18}O)$ and $\delta(^{17}O)$ values, or triple oxygen isotope composition, the $\Delta(^{17}O)$ can be calculated. This is the expression
of the deviation from a constant relation between $\delta(^{18}O)$ and $\delta(^{17}O)$ values, which can be described using an arbitrary value
defined as λ. Throughout this study we use for λ the value of 0.528, the reference line defined from measurements of $\delta(^{18}O)$
and $\delta(^{17}O)$ values in natural waters (Meijer and Li, 1998), also written as λ_{RL} and recommended as the consensus value to
40   express $\Delta(^{17}O)$ in Miller and Pack (2021).

$$\Delta'(^{17}O) = \ln(\delta(^{17}O) + 1) - \lambda_{\mathrm{RL}} \ln(\delta(^{18}O) + 1) \tag{3}$$

     The $\Delta(^{17}O)$ of tropospheric CO_2 is mainly influenced by two processes being 1) intrusion of stratospheric CO_2 carrying a
strongly deviating ($\Delta(^{17}O) >> 0$) signal (Thiemens et al., 1995; Boering et al., 2004; Kawagucci et al., 2008; Lämmerzahl
et al., 2002), due to the exchange of CO_2 and O_3 via $O(^1D)$ (Yung et al.), and 2) the equilibration of tropospheric CO_2 with
45   water, resulting in CO_2 with an $\Delta(^{17}O)$ of -0.21 ‰ (Hoag et al., 2005; Barkan and Luz, 2012), providing the water has an
$\Delta(^{17}O)$ of zero. This equilibration mainly occurs in plant leaves due to the presence of the enzyme carbonic anhydrase which
speeds up the equilibration process of CO_2 and water by order of magnitude, such that the oxygen isotope composition of CO_2
which diffuses from the leaves back into the atmosphere (about 2/3 of the total uptake of CO_2 by plants (Adnew et al., 2023))
is largely in equilibrium with that of the leaf water (Francey and Tans, 1987).

50   Measurements of stable isotopes are traditionally done with isotope ratio mass spectrometry (IRMS), however measurement
of the $\delta(^{17}O)$ of CO_2 is not straightforward with this method due to isobaric interferences of the $^{13}C^{16}O_2$ and the $^{12}C^{16}O^{17}O$

isotopologues. These measurements can therefore only be done by measuring ion fragments, requiring a higher mass resolution and a very high sensitivity IRMS system, or by O_2-CO_2 exchange, a sample preparation procedure that is very labor intensive (Mahata et al., 2013; Adnew et al., 2019). The last method mentioned is at this moment acquiring a precision higher than 0.01 ‰

55 for measurements of $\Delta'(^{17}O)$ (Adnew et al., 2019; Liang et al., 2023). Laser absorption spectroscopy measurements of $\Delta'(^{17}O)$ (next to $\delta(^{13}C)$ and $\delta(^{18}O)$) on pure CO_2 (Stoltmann et al., 2017) and directly on CO_2-in-air (Steur et al., 2021; Hare et al., 2022; Perdue et al., 2022; Bajnai et al., 2023) now reach precisions close to, or higher than the IRMS measurements. Laser absorption spectroscopy uses the absorption peaks of three different isotopologues of CO_2 to define the triple oxygen isotope composition. Therefore, the measurements can be conducted directly on air mixtures containing CO_2 at atmospheric amount fractions. This

60 strongly reduces the preparation time for $\Delta'(^{17}O)$ measurements, bringing up the potential to set-up large(r) scale measurement programs to evaluate the potential of $\Delta'(^{17}O)$ of atmospheric CO_2 for carbon cycle and atmospheric research. From 2017, the Stable Isotopes of CO_2 Absorption Spectrometer (SICAS), measuring the $\delta(^{13}C)$, $\delta(^{18}O)$ and $\Delta'(^{17}O)$ of atmospheric CO_2, has been taken into use at the Centre for Isotope Research (CIO) in Groningen. Air samples from two atmospheric measurement stations, Lutjewad and Mace Head, located at the north coast of the Netherlands and west coast of Ireland, respectively, have

65 been measured regularly at the CIO for their trace gas amount fractions and stable isotope composition over the period 2017-2022. We elaborately checked the quality of the measurements by considering the full uncertainty budget, as well as comparing atmospheric sample measurements with results derived from IRMS measurements.

In this paper multi-year records of $\Delta'(^{17}O)$ measurements conducted using laser absorption spectroscopy are presented along with the CO_2 amount fraction and $\delta(^{13}C)$ and $\delta(^{18}O)$ measurements. Observational data on the triple oxygen isotope

70 composition of ~~troposheric~~ tropospheric CO_2 have been scarcely reported in the literature so far. Earlier records of $\Delta'(^{17}O)$ measurements of atmospheric CO_2, all conducted using IRMS, have been published before from Jerusalem (Israel) (Barkan and Luz, 2012), La Jolla (USA) (Thiemens et al., 2014), Taipei (Taiwan) (Liang and Mahata, 2015), cruises on the South China Sea (Liang et al., 2017), Palos Verdes ~~insula~~ peninsula (USA) (Liang et al., 2023) and Göttingen (Germany) (Hofmann et al., 2017); the only near-by-mid-latitude measurement site. Göttingen, in central Germany, located about 400 km to the south-

75 west from the Lutjewad atmospheric measurement station, has a similar, although more continental climate and its record is therefore best comparable to Lutjewad when continental air masses are sampled.

The $\Delta'(^{17}O)$ record of Lutjewad has been compared to model simulations of the $\Delta'(^{17}O)$ signal of atmospheric CO_2 in Lutjewad as described in Koren et al. (2019). Finally, an outlook is given on how the SICAS, or laser absorption spectroscopy in general, can be used to collect data relevant for studying the $\Delta'(^{17}O)$ of atmospheric CO_2 in the future.

80 ## 2 Methods

2.1 Sampling sites

The Lutjewad atmospheric measurement station is located at the northern coast of the Netherlands, at 53° 24'N, 6° 21'E. Since 2018, Lutjewad station has been a class 2 station in the European Integrated Carbon Observation System (ICOS) network. The station is located directly behind the Wadden Sea dike, in a flat, rural area. The location allows sampling of marine (background)
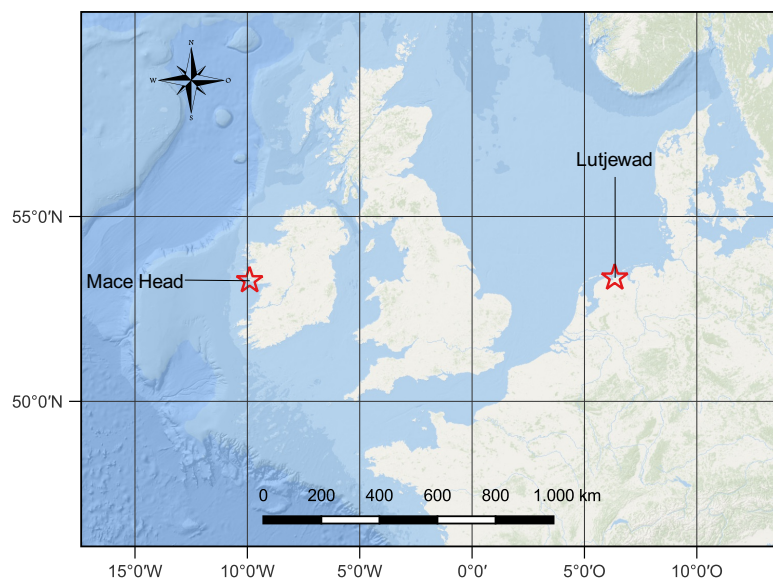
Figure 1. Locations on the map of the atmospheric measurement stations Lutjewad and Mace Head (map created by T. Maalderink)

85   air with northern winds and continental air (50 % of the time) with southerly winds. Air is pumped from the top of the 60 m high tower via inlets connected to a series of tubing towards a laboratory building containing the instruments for continuous monitoring and an automated flask sampling system. The flasks used in our flask-sampling network are 2.3 L volume glass flasks with two Louwers Hapert Viton sealed valves. The automated flask sampler is able to fill up to 20 flasks at ambient pressure and is set at a typical frequency of 1 flask sample every 3 days taken at 12:00 local time. A flask is flushed for one

90   hour with cryogenically dried sample air to a dewpoint below -50 °C before the sampler closes it and continues to flush the next flask (Neubert et al., 2004). Samples of the period 2017-2022 were used for this study. During this period occasionally the flask sampling system failed, causing periods of sparser sampling, especially during 2019 and the beginning of 2022.

    The atmospheric measurement station Mace Head, (operated by the National University of Ireland, Galway) is located at the west coast of Ireland (53° 20' N, 9° 54' W) on a cliff at 17 m above sea level. When the wind direction is from the west

95   to southwest, well-mixed air masses from the North-Atlantic cross the station (Stanley et al., 2018). These wind conditions occur about half of the time, and during these periods Mace Head can be used as a background station for Northern Hemisphere background air. Once a week, when the air masses at the site are representative for Northern Hemisphere background air, a flask sample is taken at the Mace Head station from a 23 m high tower and sent to the CIO for analysis of trace gas measurements and stable isotope composition of CO_2. From the beginning of 2019 onwards we started to routinely measure the Mace Head

100   flask samples on the SICAS.

2.2 Trace gas amount fraction measurements

Continuous measurements of CO_2, CH_4, and CO amount fractions have been conducted at the Lutjewad station with cavity ring down spectrometry (CRDS) (Picarro, G2401 series) since 2013. Flask samples were measured for the same species at the CIO laboratory, of which the majority was conducted using a customised HP Agilent HP6890N gas chromatograph (HPGC) equipped with a methaniser and a Flame Ionization Detector (Worthy et al., 2003; Laan et al., 2009) in operation until mid-2021, after which we used CRDS for flask analyses. All CO_2 measurements are calibrated using in-house made whole dry air working standards linked to the World Meteorological Organisation X2019 scale, CH_4 measurements to the X2004A scale, and CO measurements to the X2014A scale. CRDS continuous measurements are shown as hourly means and therefore the standard deviations can vary considerably, depending on the stability of trace gas amount fractions in the atmosphere during the measurement period. Flask measurements on the HPGC show typical measurement precisions of <0.1 μmol/mol, <1.0 nmol/mol, and <1.0 nmol/mol for CO_2, CH_4, and CO, respectively. In addition, CRDS measurements of the flask samples show a typical precision of <0.1 μmol/mol, <0.7 nmol/mol and <2.0 nmol/mol for CO_2, CH_4, and CO, respectively. The scale uncertainty is ±0.07 μmol/mol for CO_2, ±1 nmol/mol for CH_4, and ±2 nmol/mol for CO.

2.3 Stable isotope measurements

Stable isotope composition measurements are conducted directly on atmospheric air samples, on the same flasks collected for the trace gas amount fraction measurements, with the SICAS, a dual-laser spectrometer (CW-IC-TILDAS-D, Aerodyne) operating in the mid-infrared region. The measurement procedure is extensively described in Steur et al. (2021), and the calibration procedure and the determination of the combined uncertainty is described in chapter 5 of Steur (2023), so we only briefly explain those here. The combined uncertainty is determined for all SICAS measurements, and includes the measurement uncertainty, the repeatability and residual of the measurement series and the introduced uncertainty as a result of the calibration procedure. All these components are explained below.

Measurements are performed in static mode and are repeated for nine aliquots per sample. The gas consumption per aliquot is 20 mL, so measuring one sample requires 180 mL of air. A drift correction is carried out by measuring the working gas (a reference, being a high pressure cylinder containing air of known CO_2 amount fraction and CO_2 stable isotope composition) continuously, alternating with every aliquot measurement. This should correct the instrumental drift, that is identified also in similar measurement systems, caused by temperature variations (Hare et al., 2022; Bajnai et al., 2023). Temperature typically does not vary more than 0.05 °C within one measurement series of 12 hours for the SICAS (Steur et al., 2021). The standard error of the drift corrected aliquot measurements per sample is the measurement uncertainty. The average measurement uncertainties are 0.010, 0.009 and 0.019 ‰ for $\delta(^{13}C)$, $\delta(^{18}O)$ and $\Delta(^{17}O)$ (Steur, 2023).

Besides the flask samples and the working gas we include at least three other references in a measurement series (measurement cycle) that are all measured four times throughout the measurement series. At least two of these references, together with the working gas, are used for the calibration of the measurements. One of the references serves as a quality control (QC) measurement, or a known unknown, and is not used to determine the calibration curves but is used as an indicator for the

quality of the measurement series. The repeatability of the measurement series is calculated as the standard deviation of the four QC measurements. We observe an average repeatability of 0.03, 0.02 and 0.04 ‰ for the $\delta(^{13}C)$, $\delta(^{18}O)$ and $\Delta(^{17}O)$ per measurement series, respectively (Steur, 2023). The residual per measurement series is calculated as the average of the calibrated QC measurements minus the known value of the QC.

The calibration method used for a sample measurement depends on the CO_2 amount fraction of the sample relative to the references. The uncertainty introduced by the calibration is highly dependent on the difference, in CO_2 amount fraction, of a sample from the closest reference, as well as the difference between the references (Steur, 2023). We calibrate with the reference cylinders only, instead of having an on-line mixing facility where the reference and sample CO_2 amount fraction can be matched (Perdue et al., 2022; Bajnai et al., 2023). Therefore, samples that fall outside the range of the CO_2 amount fraction that is covered by our reference cylinders will have higher uncertainties.

We use two different calibration methods, being the isotopologue method (IM) and ratio method (RM) (Steur et al., 2021), and varying introduced uncertainties are assigned to sample measurements, depending on the difference in CO_2 amount fraction between the sample and the references. The IM is used when the sample is within the CO_2 amount fraction range of the references. For the IM quadratic calibration curves from the measured isotopologue amount fractions and known amount fractions of a minimum of three references, including the working gas, are determined. Calibrated isotopologue amount fractions of the samples are subsequently used for the calculation of the delta values. Ideally, the sample is bracketed closely in CO_2 amount fraction by the references. When the difference between the nearest reference is 15 µmol/mol or lower, uncertainties of 0.03 ‰ for $\delta(^{13}C)$ and $\delta(^{18}O)$ and 0.05 ‰ for $\delta(^{17}O)$ and $\Delta(^{17}O)$ are introduced. When the difference is higher than 15 µmol/mol, an uncertainty of 0.09 ‰ for $\delta(^{13}C)$ and $\delta(^{18}O)$ is introduced, and uncertainties of 0.11 and 0.10 ‰ are introduced for $\delta(^{17}O)$ and $\Delta(^{17}O)$, respectively.

When the sample falls outside of the CO_2 amount fraction range of the references, the RM is used. A linear correction of the measured delta values, depending on the CO_2 amount fraction is applied. In this way a correction for the introduced CO_2 amount fraction dependency of the measured delta values is applied. This correction is needed as a result of measured and assigned isotopologue amount fraction dependencies with a non-zero intercept (Griffith et al., 2012). The uncertainty increases with extrapolation distance, being the difference between the sample and the nearest reference in CO_2 amount fraction, with the sample falling outside the CO_2 amount fraction range of the references. The introduced uncertainty (u) in ‰ due to the extrapolation distance ($\Delta y(CO_2)$) in µmol/mol is determined according to the following equations:

$$
\begin{aligned}
u_{\delta(^{13}C)}/‰ &= 0.0042\Delta y(CO_2)/(\mu mol\,mol^{-1}) + 0.03 \\
u_{\delta(^{18}O)}/‰ &= 0.0054\Delta y(CO_2)/(\mu mol\,mol^{-1}) + 0.03 \\
u_{\delta(^{17}O)}/‰ &= 0.0063\Delta y(CO_2)/(\mu mol\,mol^{-1}) + 0.05 \\
u_{\Delta(^{17}O)}/‰ &= 0.0042\Delta y(CO_2)/(\mu mol\,mol^{-1}) + 0.05
\end{aligned}
\tag{4}
$$

The introduced uncertainties are all based on the empirical data of reference measurements over a period of two to three years, as described in Chapter 5 of Steur (2023). As the Lutjewad and Mace Head stable isotope records presented in this study

are measured only on the SICAS, scale uncertainties are not included in the combined uncertainties of the measurements.
To prevent showing irrelevant results, only values with a combined uncertainty lower than 0.1 ‰ will be included in the results of the stable isotope measurements. The highest reference included in the calibration for the records has a CO_2 amount fraction of 424.54 µmol/mol, so the consequence is that samples with CO_2 amount fractions higher than 441.2, 437.5 and 436.4 µmol/mol are excluded from the $\delta\delta(^{13}C)$, $\delta(^{18}O)$ and $\Delta^{2}(^{17}O)$ records, respectively. Especially at the Lutjewad station it is not uncommon to sample air in this range of CO_2 amount fractions during winter. This will hence lead to a bias, as results of local or regional events leading to elevated CO_2 amount fractions that were captured in the flask records are not included in the results. Extending the CO_2 amount fraction range of our reference cylinders will improve the measurement precision of samples with elevated CO_2 amount fractions, as well as extend the range of CO_2 amount fractions that can be shown in the results. A way to prevent that a high number of reference cylinders has to be included at all times, is to make the selection of references more dynamic. As sample measurements are always alternated with a working gas measurement, it is possible to do a 1-point calibration immediately after a sample is measured. In this way it will be possible to select the ideal set of references to calibrate the samples based on the CO_2 amount fractions derived from the 1-point calibration. This would save reference gas, as well as measurement time of a measurement series.

Table 1. Natural air references used for the calibration of stable isotope measurements presented in this study. $\delta(^{13}C)$ and $\delta(^{18}O)$ values as measured at the BGC-IsoLab. $\Theta\theta_{IMAU}$ is the $\delta(^{17}O)$-$\delta(^{18}O)$ relation as measured at IMAU. $\delta(^{17}O)$ and $\Delta^{2}(^{17}O)$ are calculated from the $\delta(^{18}O)$ and $\Theta\theta_{IMAU}$. Values indicated with * are derived from SICAS measurements as these references were not measured at the IMAU. Uncertainties include the measurement uncertainty, repeatability and accuracy.

	yCO_2 / µmol mol^{-1}	$\delta(^{13}C$, VPDB) / ‰	$\delta(^{18}O$, VSMOW) / ‰
Reference 1	405.96 ±0.03	-8.63± 0.013	37.269±0.018
Reference 2	417.27±0.02	-9.13±0.019	38.102±0.018
Reference 3	424.71±0.005	-9.438± 0.016	37.69±0.03
Reference 4	413.61	-8.99±0.012	36.884±0.019
Reference 5	343.12±0.02	-9.4±0.007	37.689±0.017
Reference 6	399.17	-8.22±0.02	37.595±0.04
Reference 7	379.01±0.05	-7.52±0.013	40.05±0.02
	θ_{IMAU}	$\delta(^{17}O$, VSMOW) / ‰	$\Delta(^{17}O)$ / ‰
Reference 1	0.5218	19.280±0.019	-0.224±0.019
Reference 2	0.5215	19.693±0.018	-0.243±0.018
Reference 3	0.5216	19.49±0.03	-0.24±0.03
Reference 4	n.a.	19.08*±0.06	-0.22*±0.05
Reference 5	0.5211	19.464±0.018	-0.256±0.018
Reference 6	n.a.	19.44*±0.06	-0.23*±0.05
Reference 7	n.a.	20.72*±0.15	-0.23*±0.10

For calibration of the SICAS isotope measurements we use the in-house produced gas references, consisting of dried atmospheric air in high pressure gas cylinders, as presented in table 1. The CO_2 amount fractions of the references were measured on a PICARRO G2401 gas amount fraction analyzer and calibrated using in-house working standards, linked to the WMO 2019 scale for CO_2 with a suite of four primary standards provided by the Earth System Research Laboratory of the National Oceanic and Atmosphere Administration (NOAA).

To ensure cylinders drifting in CO_2 amount fraction are identified, all reference cylinders are measured on the PICARRO once a year. The uncertainty of the CO_2 amount fractions in table 1 is the standard error of those measurements through the years. Considering the low standard errors ranging between 0.005-0.05 µmol/mol there are no signs of drifting CO_2 amount fractions in any of the cylinders. Cylinders 4 and 6 were only measured once, so no standard errors are shown in table 1.

Aliquots of all references have been analyzed at the stable isotope lab of the Max Planck- Institut for Biogeochemistry in Jena (BGC-IsoLab) by DI-IRMS to link the $\delta(^{13}C)$ and $\delta(^{18}O)$ directly to the JRAS-06 scale (Jena Reference Air Set for isotope measurements of CO_2 in air (VPDB(-CO_2) scale)) (Wendeberg et al., 2013). Stable isotope composition of the reference gases measured at the BGC-IsoLab and the standard errors of the measurements (standard error of the results of all aliquot measurements) are presented in table 1.

Despite the existence of this direct linkage of atmospheric CO_2 to the VPDB-CO_2 scale, triple oxygen isotope measurements of atmospheric CO_2 are usually expressed on the VSMOW scale (Hofmann et al., 2017; Adnew et al., 2020; Boering et al., 2004). Also, an internationally recognized isotope scale for $\delta(^{17}O)$ has so far not been established. It is therefore not straightforward to determine the $\delta(^{17}O)$ values of our reference cylinders ourselves. We use the $\delta(^{18}O)$ values measured at BGC-IsoLab in combination with triple oxygen isotope measurements of references 1-3 and 5 conducted at the Institute for Marine and Atmospheric research Utrecht (IMAU), using the O_2-CO_2 exchange method and DI-IRMS measurements (Adnew et al., 2019). The measured θ of the references, calculated as $\ln(\delta(^{17}O)+1)/\ln(\delta(^{18}O)+1)$, from now on defined as θ_{IMAU}, was used to calculate $\delta(^{17}O)$ values on the VSMOW scale from the $\delta(^{18}O)$ values as measured by BGC-IsoLab. The latter were converted from VPDB-CO_2 to VSMOW by the following equation, as recommended in Hillaire-Marcel et al. (2021):

$$\delta_{VSMOW}(^{18}O) = 1.04149 \cdot \delta_{VPDB\text{-}CO_2}(^{18}O) + 41.49\,\%o \tag{5}$$

Next the following equation was applied to the BGC-IsoLab $\delta(^{18}O)_{VSMOW}$ values:

$$\delta_{VSMOW}(^{17}O) = (\delta_{VSMOW}(^{18}O) + 1)^{\theta_{IMAU}} - 1 \tag{6}$$

$\Delta(^{17}O)$ values were calculated by applying the $\delta(^{18}O)_{VSMOW}$ and $\delta(^{17}O)_{VSMOW}$ values to equation 3. For the references that were not measured at the IMAU, the $\delta(^{17}O)$ values were determined from SICAS measurements, using the calibration methods and uncertainty assignment as described before. The $\Delta(^{17}O)$ was subsequently calculated using this measured $\delta(^{17}O)$, and the $\delta(^{18}O)$ as measured by the BGC-IsoLab. Note that the scale described above for the $\Delta(^{17}O)$ values is indirectly linked to VSMOW, adding uncertainty to the compatibility of other $\Delta(^{17}O)$ scales.

For measurement of our reference gases by the BGC-IsoLab and IMAU, aliquots were prepared by connecting 5 sample flasks in series and flush them with the sample gas, resulting in a similar air sample in all flasks. However, deviations of the

sampled air from the air in the reference cylinders as the result of alterations of the gas inside the flasks can be introduced (Steur et al., 2023).

2.4 Comparison CIO and IMAU

For a selection of Lutjewad samples two flasks containing identical air were sampled (from now defined as a duplicate) of which one flask was measured at the CIO, using laser absorption spectroscopy, and one at the IMAU, using DI-IRMS, to check the compatibility of the two methods. From 2019 a fully automatic extraction system has been taken into use at the IMAU which enables to extract CO_2 from air and directly analyse the sample on their DI-IRMS. Before that time, extraction of CO_2 from the air samples was done at the CIO and the pure CO_2 samples were sent to the IMAU in flame sealed tubes for DI-IRMS analysis.

The $\delta(^{13}C)$ sample differences are higher than expected from the combined uncertainty of the SICAS measurements, as can be seen in figure 2. The frequency distribution shows that at least part of the differences are because of systematic errors, possibly scaling or sampling issues. It should be noted that the quality of the SICAS measurements is lower for the samples measured at the end of 2019 and in 2020. Samples from 2018, from which the CO_2 was extracted at the CIO, show a positive offset of the SICAS measurements relative to the IMAU measurements. A reason for the building up of differences in $\delta(^{13}C)$ values during that period has not been found.

Results of the differences of the $\delta(^{18}O)$ measurements are shown in Appendix A1. The differences are far outside the uncertainty range of the SICAS measurements, being up to 2 ‰. These high differences are connected to the observations of drift in the oxygen isotopes of CO_2 in flask samples as a function of time (Steur et al., 2023). $\Delta'(^{17}O)$ values are not (or hardly) affected by the drifts in oxygen isotopes in the flasks. We calculated that, in the extreme case of a change of more than 3 ‰ in $\delta(^{18}O)$ of atmospheric CO_2 (Steur, 2023) resulting from equilibration of CO_2 with water inside the flask, and at the same time an initial $\Delta'(^{17}O)$ value of the CO_2 of -0.69 ‰, changes the $\Delta'(^{17}O)$ less than 0.06 ‰. Considering that the uncertainty of the SICAS $\Delta'(^{17}O)$ measurements is always 0.05 ‰ or higher, we can conclude that the effect of drift of the oxygen isotopes inside the flasks is negligible for the $\Delta'(^{17}O)$ values. Results and calculations that support this conclusion can be found in Appendix B1.

The $\Delta'(^{17}O)$ differences fall in general within the mean combined uncertainty of the SICAS measurements over the whole sampling period. The total range of $\Delta'(^{17}O)$ of the samples is, however, small, being 0.15 ‰. Nevertheless, this comparison shows that the CIO calibration procedure gives $\Delta'(^{17}O)$ values similar to IMAU, and the repeatability of the measurements falls within the combined uncertainty of the SICAS measurements. The differences are normally distributed so there are no systematic offsets between the two labs.

In Appendix C we elaborate further on the comparison of $\Delta'(^{17}O)$ measurements and also the complete record of Lutjewad $\Delta'(^{17}O)$ measurements, including all IMAU measurements is shown (figure C2). This figure shows that the variation that is observed in the IMAU measurements coincides with variation that is observed from the SICAS measurements.
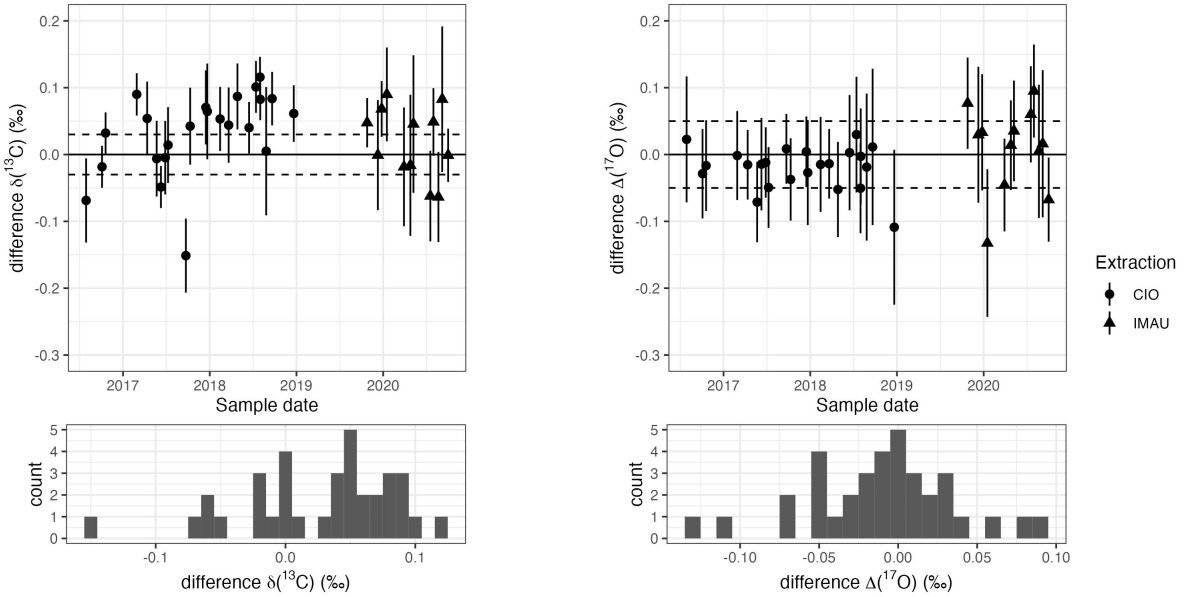
Figure 2. The top panels shows the differences (CIO-IMAU) of $\delta(^{13}C)$ and $\Delta^2(^{17}O)$ measurements of the duplicate flasks. Uncertainty bars show the combined uncertainty (+/- 1-σ), as defined is section 2.3, of the CIO measurements. Shape of the data points indicates whether CO_2 was extracted at CIO and send to IMAU as pure CO_2 samples (circles) or whether extraction was done at IMAU (triangles). The lower panels shows the frequency distribution of the differences.

2.5 Atmospheric modeling of $\Delta^2(^{17}O)$ in CO_2 at Lutjewad

In addition to the measurements, we present model simulations for $\Delta^2(^{17}O)$ in CO_2 for the Lutjewad location by the 3-D
245 transport model described in Koren et al. (2019). As the Mace-Head and Lutjewad latitude is similar, we do not expect to see significant differences of simulations between the two locations. The model includes the stratospheric input of high $\Delta^2(^{17}O)$ and processes that will lead to reduction of the stratospheric signal, being biosphere activity, equilibration of CO_2 with soil moisture, CO_2 emissions from fossil fuel and biomass burning and CO_2 uptake and emission from the oceans. An update to this model is the use of meteorological driver data from the ERA5 release (Hersbach et al., 2020), instead of the ERA-Interim
250 fields (Dee et al., 2011) that were used previously. The model resolution applied for the Lutjewad simulation is a longitude-latitude grid of 1° by 1°. Here we present simulations for $\Delta^2(^{17}O)$ in CO_2 for the years 2017 until the end of 2021. Note that the long-term mean values simulated by the model for Lutjewad are ultimately dependent on the integrated contribution from all processes across the globe, which are poorly constrained in the model (e.g. due to large uncertainties in soil exchange, see Wingate et al. (2009)). Therefore we focus on the timing and amplitude of the seasonal cycle and the interannual variability of
255 $\Delta^2(^{17}O)$ in CO_2 at the Lutjewad station.

3 Results and discussion

3.1 CO_2 amount fraction measurements results

In figure 3 the CO_2 amount fraction measurements of the Lutjewad and Mace Head flasks measured at the CIO over the period 2017-2022 are shown, together with the continuous CO_2 amount fraction measurements from Lutjewad. As an independent comparison, the Mace Head CO_2 amount fraction measurements of discrete air samples from the NOAA-Global Monitoring Laboratory Carbon Cycle Greenhouse Gases cooperative air sampling network (NOAA-GML CCGG) (Lan et al., 2022) are plotted in the same figure. The Mace Head flask samples measured at the CIO are in good agreement (within precision) with the overlapping time series results from the NOAA-GML CCGG. A background CO_2 amount fraction curve has been determined from the Lutjewad continuous CO_2 amount fraction measurements. This was done by including only measurements of samples taken during daytime (between 10:00 and 19:00 UTC) and excluding hourly averages with standard deviations higher than 0.5 µmol/mol and CO values higher than 140 nmol/mol. Subsequently, the filtered signal was smoothed by a moving average of 30 points and the result was fitted with a quadratic trend with a 2-harmonic seasonality. The resulting background signal, shown in figure 3 as the black line, corresponds well with the Mace Head measurements. This confirms that the derived background curve represents well-mixed air, not influenced by local contamination events from fossil fuel burning. This CO_2 amount fraction background curve is used in the stable isotope records to calculate the $\Delta_{bg}\chi(CO_2)$ of a sample, being the difference in amount fraction between the sample and the background curve.

The background curve shows the strong influence of the biosphere, resulting in CO_2 amount fractions that are almost 15 µmol/mol lower in summer than in winter. The seasonality shows maxima at the beginning of the growing season in March and April and minima at the end of the growing season in August. The overall increase of CO_2 amount fractions in the atmosphere is clearly visible from the background curve and is 2.5 µmol/mol per year. These results are very close to growth rate of the globally averaged CO_2 amount fractions of 2.4 µmol/mol per year (standard deviation 0.5 µmol/mol per year) from 2011 to 2019 (Friedlingstein et al., 2022).

The Lutjewad flasks, although sampled at noon with the aim to sample well-mixed tropospheric air, occasionally show large positive deviations from the background curve, especially in winter, of up to +47 µmol/mol in December 2017. The CO_2 enriched signals are most probably due to local and regional sources of CO_2, either natural or anthropogenic, that occur on the continent. We therefore expect to see more deviations from the seasonal cycles of stable isotope values induced by the more continental influence at the Lutjewad record when compared to the Mace Head record.

The Europe wide drought, which was most severe in Northern Europe, during the summer of 2018 (Peters et al., 2020; Ramonet et al., 2020) is clearly visible in the continuous CO_2 amount fraction record of Lutjewad, where a short-term increase in CO_2 amount fractions interrupts the overall decrease in amount fractions that normally occurs over the growing season. In early spring of 2018, CO_2 amount fractions decrease rapidly (when the growing conditions were more favorable, see Smith et al., (2020)), until May 2018. Subsequently a rapid increase in CO_2 amount fractions is observed that lasts until June, before CO_2 amount fractions start decreasing again. This event is only visible in one Lutjewad flask sample having a $\Delta_{bg}\chi(CO_2)$ of -8.6 µmol/mol and two Mace Head samples from the NOAA-GML CCGG having $\Delta_{bg}\chi(CO_2)$'s of -6.7 and -7.1 µmol/mol.

Due to the too low sampling frequency, the drought event is hard to identify from the flask samples only. In 2022 Europe experienced another severe drought, which was, however, mostly located in central and southeastern Europe (van der Woude et al., 2023). This drought event does not show up in the continuous amount fraction record of Lutjewad as observed for the 2018 drought.

Figure 3. CIO CO_2 amount fractions from continuous measurements shown as hourly averages and discrete flask sample measurements of the Lutjewad atmospheric measurement station, and discrete flask sample measurements from the Mace Head atmospheric measurement station from the NOAA GML Carbon Cycle Cooperative Sampling Network and the CIO. The seasonal cycle (black line) is derived from the filtered continuous measurements that were fitted with a quadratic trend with a 2-harmonic seasonality.

3.2 Stable isotope measurements

Results of $\delta(^{13}C)$ measurements on atmospheric CO_2 of discrete flask samples from Lutjewad and Mace Head are shown as a function of sampling date in figure 4. A quadratic trend with a 2-harmonic seasonality is fitted on all Lutjewad $\delta(^{13}C)$ points that have a $\Delta_{bg}y\chi(CO_2)$ that is not higher than 5 µmol/mol. There are too few data points for doing a fit on the Mace Head record. Instead, the Lutjewad seasonal trend is also plotted in the Mace Head record so both records can be easily compared. The seasonality in the $\delta(^{13}C)$ records shows a strong anti-correlation with the CO_2 amount fraction records, with maxima during late summer, and minima in late winter. During winter, there are negative excursions in the Lutjewad record that do not appear in the Mace Head record, from which we can conclude that the Lutjewad $\delta(^{13}C)$ is influenced by more local or regional signals resulting in more depleted $\delta(^{13}C)$ signals like fossil fuel emission and plant and soil respiration (Keeling et al., 2017; Scholze et al., 2008). For the same reason, the seasonal curve derived from the Lutjewad data shows a stronger decrease of $\delta(^{13}C)$ values in Autumn and Winter than the Mace Head record. When Lutjewad would be more influenced by the strong biosphere activity at the continent, heavier (i.e. less negative) $\delta(^{13}C)$ values than at Mace Head would be expected during the summer. For the year 2020 and 2021 this is the case, but in 2019 the Mace Head values are heavier. The year 2019 is, however, a period in which Lutjewad samples were collected more sparsely due to problems with the sampling system. It is therefore hard to conclude whether there is in general a heavier $\delta(^{13}C)$ signal in Lutjewad compared to Mace Head during the summers. Overall, a decreasing trend is observed from the seasonal fit, explained by the increase in CO_2 amount fractions in the atmosphere due to the combustion of fossil fuels, also known as the ^{13}C Suess effect (Keeling, 1979).

Measurements of $\delta(^{18}O)$ of atmospheric CO_2 from Lutjewad and Mace Head flask measurements conducted at the SICAS are presented in figure 5. A seasonal curve is fitted from the Lutjewad data using the same method as for the $\delta(^{13}C)$ data. The Mace Head observations coincide with the Lutjewad fit, with maxima in May and June and minima in December and January. Although the maximum and minimum values are very similar, the maximum values in Mace Head during the summer of 2022 are more enriched than the Lutjewad values. These differences might be explained by the difference in $\delta(^{18}O)$ composition of the source waters for the vegetation at both sites (Levin et al., 2002). It should be noted that a great part of the $\delta(^{18}O)$ values
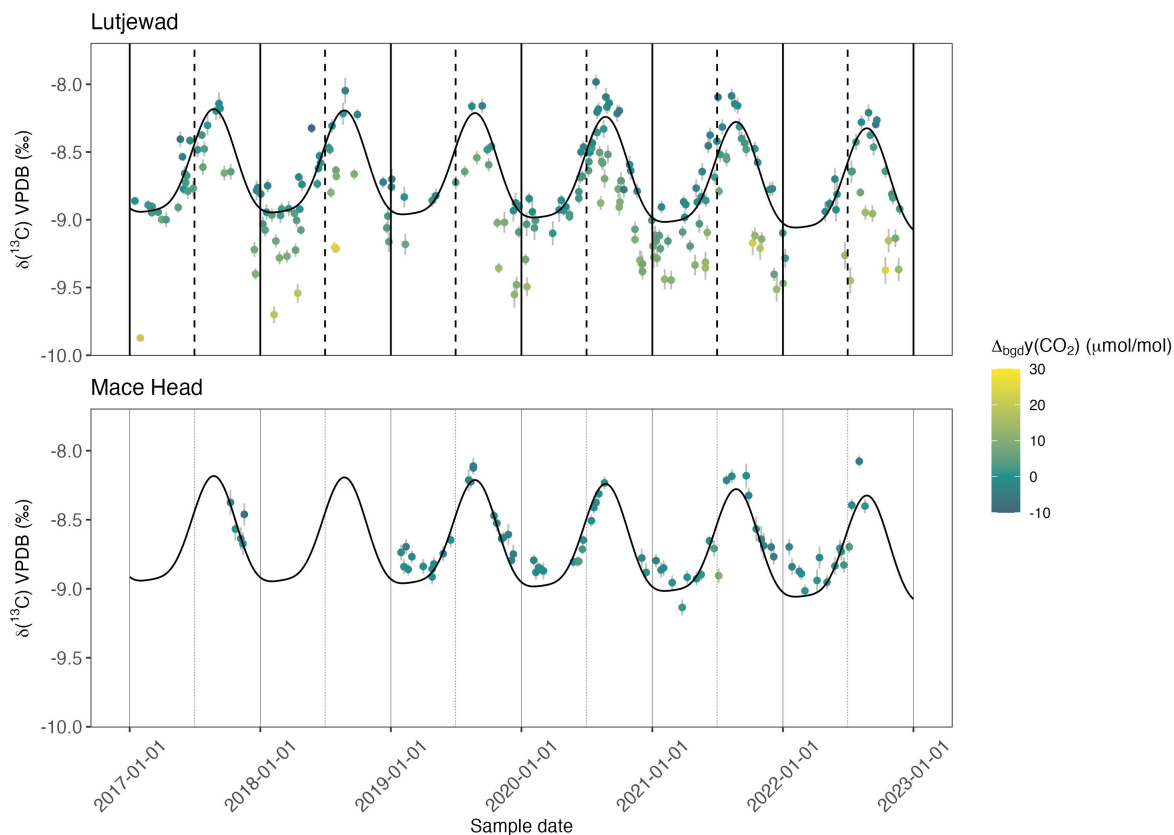
Figure 4. $\delta(^{13}C)$ records of Lutjewad and Mace Head from SICAS flask measurements of atmospheric CO_2. The upper graph shows $\delta(^{13}C)$ measurements from Lutjewad, the lower graph from Mace Head. The combined uncertainty of the measurements is shown as the grey error bars (+/- 1-σ) and include measurement uncertainty, repeatability and accuracy and introduced uncertainty as a consequence of the calibration method used. $\Delta_{bg}\gamma(CO_2)$ is indicated by the colour of the data points. The seasonality curve is derived from fitting the Lutjewad $\delta(^{13}C)$ values of samples that have a $\Delta_{bg}\gamma(CO_2)$ not higher than 5 μmol/mol and is shown as the black line in both graphs (the Lutjewad seasonal curve is also shown in Mace Head graph). The fitting method that was used is the same as for the CO_2 background curve.
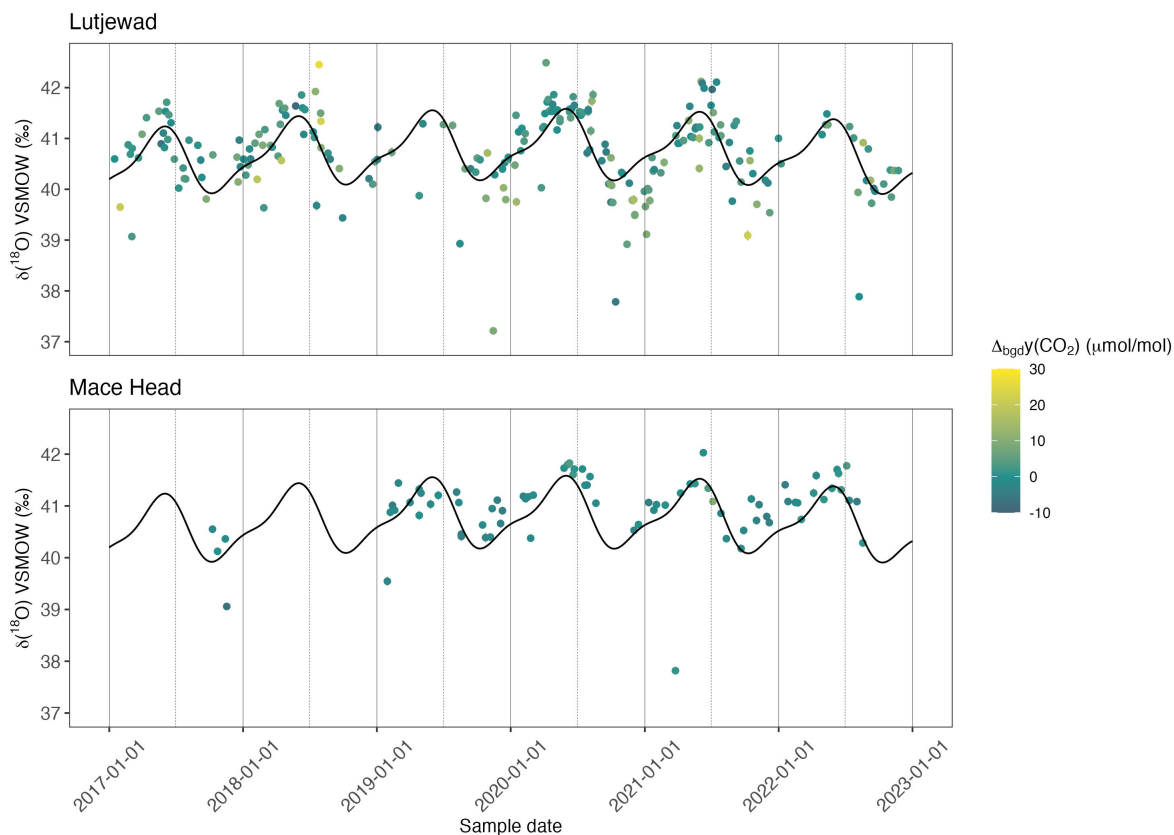
Figure 5. $\delta(^{18}O)$ records of Lutjewad (upper graph) and Mace Head (lower graph) from SICAS flask measurements of atmospheric CO_2. The combined uncertainties are shown as the grey error bars (+/- 1-σ) and include measurement uncertainty, repeatability and accuracy and introduced uncertainty as a consequence of the calibration method used. $\Delta_{bg}y(CO_2)$ is indicated by the colour of the data points. The seasonality curve is derived from fitting the Lutjewad $\delta(^{18}O)$ values of samples that have a $\Delta_{bg}y(CO_2)$ not higher than 5 µmol/mol and is shown as the black line in both graphs (the Lutjewad seasonal curve is also shown in Mace Head graph). The fitting method that was used is the same as for the CO_2 background curve.

Figure 6. $\Delta'(^{17}O)$ records of Lutjewad (upper graph) and Mace Head (lower graph) from SICAS flask measurements of atmospheric CO_2. The combined uncertainties are shown as the grey error bars (+/- 1-σ) and include measurement uncertainty, repeatability and accuracy and introduced uncertainty as a consequence of the calibration method used. $\Delta_{bg}y(CO_2)$ is indicated by the colour of the data points. Model simulations for Lutjewad (Koren et al., 2019) showing daily values at 13:00 UTC are shown in the upper graph as the black line.

of the atmospheric CO_2 samples shown here are likely to have a bias towards depletion, due to the drift we observe over time, explained in section 2.4. Interpretation of the absolute changes in the $\delta(^{18}O)$ values should therefore be done with caution, taking the storage time into account.

320    $\Delta'(^{17}O)$ measurements from the Lutjewad and Mace Head stations are presented in figure 6. The total range in the Lutjewad and the Mace Head record is 0.5 and 0.2 ‰, respectively, with an average combined uncertainty of the measurements of 0.07 ‰ for both records. Following ~~Hoag~~ Koren et al. (~~2005~~2019) we would expect to see a seasonality of increasing $\Delta'(^{17}O)$ values over winter and decreasing values over summer, when the biosphere is most active. We plotted the $\Delta'(^{17}O)$ against 1/CO_2 amount fraction and $\delta(^{13}C)$ for summer and winter values of Lutjewad (see figure Appendix D1). Mace Head was excluded
325   from this analysis as the many data gaps over the measurement period would not give a representative result. If seasonality resulting from the biosphere activity would be present this should show up in the plots as a distinction in $\Delta'(^{17}O)$ summer and winter values. Also correlations between the $\Delta'(^{17}O)$ and the 1/CO_2 and $\delta(^{13}C)$ would be expected, as the latter two also follow this seasonality. We did not observe any of this, indicating there is no significant seasonality caused by the biosphere signal in our Lutjewad $\Delta'(^{17}O)$ record. This differs from results from the Göttingen record over the period 2010-2012, where a
330   seasonality was observed with maximum values during June and July (Hofmann et al., 2017). The amplitude of the seasonality that was determined from the Göttingen $\Delta'(^{17}O)$ record is (0.13$\pm$0.02) ‰. If such a seasonality would be present in the Lutjewad and Mace Head record, we would expect to see it, as this signal is higher than the average combined uncertainty of the SICAS measurements. It can be, that due to the more continental location, the amplitude of the $\Delta'(^{17}O)$ seasonality is higher at the Göttingen site reflecting a stronger biosphere signal. A model simulation of the Göttingen location shows an amplitude
335   of 0.045 ‰ (Hofmann et al., 2017), while the amplitude of the simulation at the Lutjewad location, shown as the black line in figure 6 is close to 0.025 ‰. The model used in the Hofmann paper (2017) is an earlier version of the model used in this study (Koren et al., 2019), so the results should be well comparable. The higher amplitude for the simulation of the Göttingen location confirms the hypothesis of a higher $\Delta'(^{17}O)$ seasonality due to the more continental location in comparison with Lutjewad. It is unlikely that a considerably lower seasonal signal than observed at the Göttingen location would be detected by the SICAS
340   measurements considering their average combined uncertainties.

The low sampling frequency in combination with the sampling method at both locations will complicate capturing small seasonal variations. Air samples represent only a snapshot in time, while at the same time the frequency of sampling is only once every 3 days (Lutjewad) or even once every week (Mace Head) (Nevison et al., 2010). Changing the sampling method to a method in which the sampled air evenly represents a certain sampling period, would decrease the influence of short variability

345 in the atmospheric composition at the sampling site (Chen et al., 2012). To get a much higher sampling frequency for $\Delta^2(^{17}O)$ measurements at Lutjewad in the future, our laser absorption spectroscopy system will be deployed in the (semi-)continuous measurement mode, a technique already shown by Kaiser et al. (2022). This will enable us to apply rigid filtering on the data to derive either results representative of well-mixed background air, or, on the other hand, results that are representative for air masses from the continent.

350 The most important difference between the Lutjewad and Mace Head $\Delta^2(^{17}O)$ records is the presence of more depleted values in the Lutjewad record, with the lowest value being -0.43 ‰ in the summer of 2022. CO_2 equilibrated with water following λ_{RL} will have an $\Delta^2(^{17}O)$ of -0.21 ‰. In summer, leaf water gets enriched in oxygen isotopes, and depleted in $\Delta^2(^{17}O)$ as the result of high rates of evapotranspiration (Landais et al., 2006). Due to the active biosphere during summer, CO_2 and leaf water will equilibrate and the depleted $\Delta^2(^{17}O)$ signal will be translated to the CO_2 (Adnew et al., 2023). We

355 estimated that this could result in $\Delta^2(^{17}O)$ values being up to 0.1 ‰ more depleted, when assuming the minimum Θ θ of 0.516 for evapotranspiration (Landais et al., 2006), and considering the range of $\delta(^{18}O)$ values that were measured in our Lutjewad record. For the full estimation we refer to Appendix E. $\Delta^2(^{17}O)$ values down to -0.31 ‰ can be explained by this process. CO_2 emitted from combustion processes has very negative $\Delta^2(^{17}O)$ values (Laskar et al., 2016; Horváth et al., 2012). All points that have lower $\Delta^2(^{17}O)$ than -0.3 ‰, and are sampled during winter/spring, have more depleted $\delta(^{13}C)$ values and more enriched

360 CO_2 values than would be expected from the seasonal trends. This indicates that local CO_2 emission sources are the reason for the more depleted $\Delta^2(^{17}O)$ values in winter. Samples that are very enriched in CO_2 amount fractions are not shown here, as these results have very high measurement uncertainties. This could be the reason that a correlation of $\Delta^2(^{17}O)$ and CO_2 amount fractions does not appear in figure D1. A few points show depletions lower than -0.31 ‰ without CO_2 amount fraction enrichments, and remain for now unexplained.

365 Significant differences of $\Delta^2(^{17}O)$ values over time are observed in both records. In the Lutjewad record we observe $\Delta^2(^{17}O)$ values that are above or close to -0.2 ‰ at the beginning of 2020. Then values decrease until reaching minimum values in October 2020 with the lowest value in that period being -0.34 ‰. An increase of $\Delta^2(^{17}O)$ values is observed after this period and May 2021 is a period with more elevated values, with the highest observation being -0.09 ‰. Although the Mace Head record shows gaps over the period from 2020-2021, it is clear that values at the beginning of 2020 are higher than at the end

370 of 2020. This interannual variability in both records indicates that other processes than biosphere activity cause most of the variation at the measurement locations.

3.3 Sensitivity analysis simulated $\Delta^2(^{17}O)$ interannual variability

The total variation predicted by a local simulation of the model (base version in Koren et al., 2019) for the location of Lutjewad is lower than the uncertainty and variability of the SICAS measurements, and has a seasonal character only. The model simu-

375 lation of $\Delta^2(^{17}O)$ of atmospheric CO_2 is shown for the Lutjewad mid-latitude band as the black line in figure 6. Daily values at 13:00 UTC (corresponding to 14:00 or 15:00 local time) are shown, that thus represent well-mixed afternoon conditions, which are typically more reliable in relatively coarse global models than simulated nighttime or early morning values. Although small, there is a clear seasonality with highest $\Delta^2(^{17}O)$ values in early spring when stratospheric influx is highest with low biospheric

activity aggregated over the preceding months, and lowest values during early autumn, when the biospheric carbon uptake has depleted the tropospheric $\Delta^2(^{17}O)$ budget. Values are all between -0.16 and -0.21 ‰ which is significantly narrower than the observed range at Lutjewad. It is therefore clear that the current model version does not capture the variation in $\Delta^2(^{17}O)$ that is measured at the Lutjewad record. The Göttingen record (Hofmann et al., 2017) also shows significant interannual changes in $\Delta^2(^{17}O)$ values of 0.1 ‰, which have not been explained so far. In that record, spanning the period from June 2010 until August 2012, they found a negative shift in the $\Delta^2(^{17}O)$ values from the summer of 2011 until the end of the record.

The biosphere sink of $\Delta^2(^{17}O)$ cannot cause the interannual changes in the records since then a stronger or weaker seasonal cycle is also expected to occur. The variations observed in the Lutjewad and Mace Head records is furthermore driven by anomalies in multiple seasons and not limited to summer or winter periods only. Besides the biospheric sink, the other main term in the $\Delta^2(^{17}O)$ budget is its stratospheric production and downward transport. We therefore hypothesize that the stratospheric input of $\Delta^2(^{17}O)$ is not well parameterized in the model, leading to the limited interannual variability that is simulated in figure 6.

In the 3-D atmospheric model the stratospheric production of $\Delta^2(^{17}O)$ of atmospheric CO_2 is implemented using its empirical relation with stratospheric N_2O amount fractions (see Sect. 2.2 in Koren et al., 2019, for a more detailed description), shown in the equation below

$$\Delta_{\mathrm{fit}}(^{17}O) = a(y_{\mathrm{dtd}}(N_2O) - 320.84 \,\mathrm{nmol/mol}) + b \tag{7}$$

where $\Delta_{\mathrm{fit}}(^{17}O)$ is the assigned stratospheric signature, $[N_2O]_{\mathrm{dtd}}$ is the detrended N_2O amount fraction, and a and b are empirical fit coefficients. The N_2O amount fraction in the stratosphere and the $\Delta^2(^{17}O)$ in CO_2 are negatively correlated, based on measurements from four different studies, as presented in Koren et al. (2019). The use of this relation as the only driver for the $\Delta^2(^{17}O)$ source from the stratosphere is very coarse and it is possible that factors such as temperature, as postulated by Wiegel et al. (2013), have an effect on the $\Delta^2(^{17}O)$ enrichment of CO_2 in the stratosphere.

To increase variability in the simulated stratospheric production of $\Delta^2(^{17}O)$, we included an additional empirical production term for the region 60-90° N in winter based on 100 hPa temperature anomalies (over this same period and region) from the National Centers for Environmental Prediction (NCEP). Temperature at 100 hPa at 60-90° N, or lower stratosphere temperature, is shown to be a proxy for stratosphere-troposphere exchange during the months January-March, as it is linked to the strength of the polar vortex, which negatively correlates with the strength of the Brewer-Dobson circulation (Newman et al., 2001; Nevison et al., 2007). The Brewer-Dobson circulation is the meridional circulation driven by large-scale temperature gradients on earth leading to ascending air near the tropics and subsidence of air near the poles. A strong Brewer-Dobson circulation will lead to higher volumes of stratospheric air intruding into the troposphere during winter, as the polar vortex is then weaker (Nevison et al., 2007). This links the lower stratosphere temperature during the Northern-Hemisphere winter to the strength of the input of CO_2 with a high $\Delta^2(^{17}O)$ composition into the troposphere. The adjusted $\Delta^2(^{17}O)$ production term is defined as

$$\Delta_{\mathrm{source}}(^{17}O) = \overbrace{a(y_{\mathrm{dtd}}(N_2O) - 320.84 \,\mathrm{nmol/mol}) + b}^{\text{original production term}} + \overbrace{c\Delta T_{100\mathrm{hPa}}}^{\text{added term}} \tag{8}$$
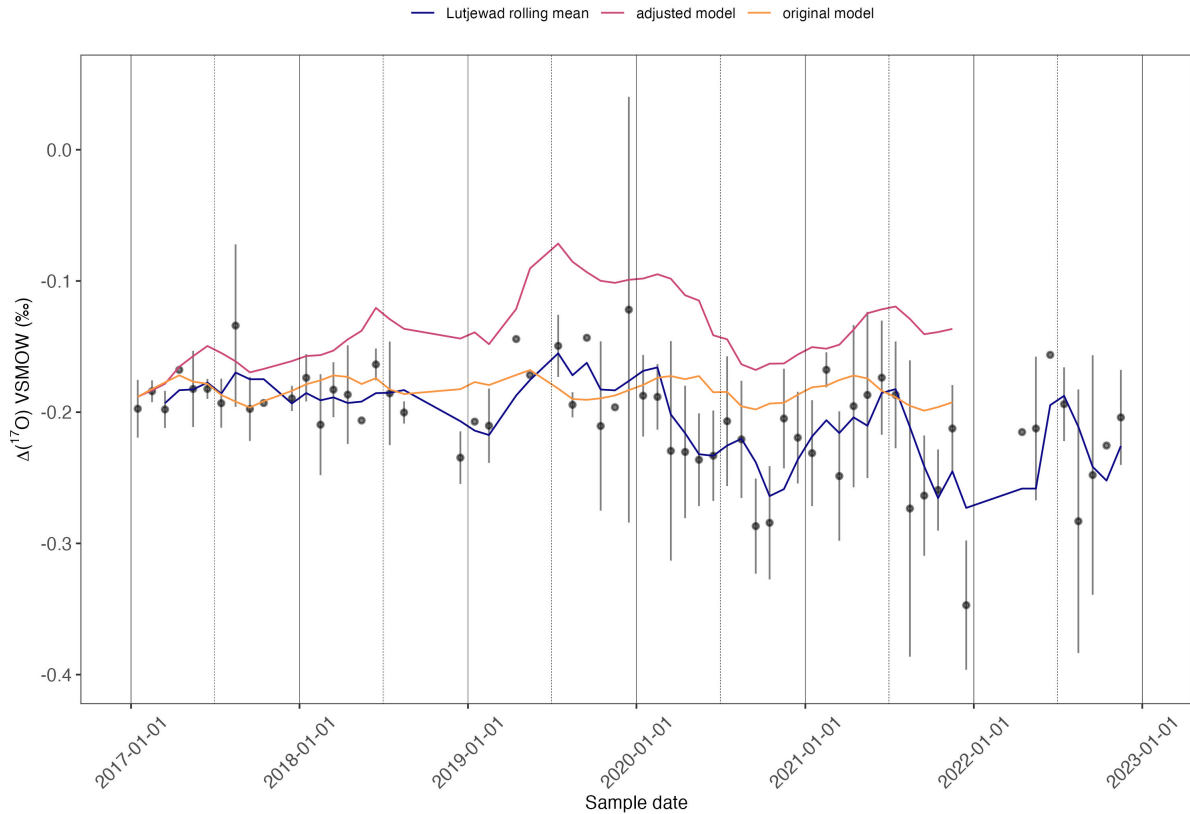
Figure 7. In black dots the monthly averages of the Lutjewad $\Delta^2(^{17}O)$ record, the error bars show the standard deviation (+/- 1-σ) of all values per month. Plotted lines are the Lutjewad rolling mean (window=3), the original model simulation (as described in (Koren et al., 2019) and the monthly averages of the adjusted model simulation in which the input of $\Delta^2(^{17}O)$ into the troposphere is linked to the lower stratosphere temperature.

where the first part is repeated from equation 7, and the added last term describes the imposed coupling with temperature anomalies at the 100-hPa level ΔT_{100hPa} with c being a tunable parameter. Here, the empirical parameters a, b and c are constant for a given simulation, whereas the $[N_2O]_{dtd}$ value differs for each grid point and with time. The temperature anomaly ΔT_{100hPa} is determined by taking the average temperature of the months January, February and March at 100 hPa for 60-90° N

415 per year for the period 2017-2022. Subsequently the difference between these values and the average of all 6 years is calculated. In equation 7 it is set to zero for regions below 60° N and for months April-December. Note that ~~the temperature~~ both the N_2O amount fractions and the temperature anomaly are used as proxy values for the $\Delta(^{17}O)$ value in the stratosphere. Thereby, the temperature relation represents both temperature dependence of the actual $\Delta^2(^{17}O)$ as suggested in Wiegel et al. (2013) and the temperature dependence in stratospheric exchange, which might not be sufficiently represented with only 25 vertical layers in

420 the current model (see e.g. Bândă et al., 2015, for the influence of vertical resolution on stratosphere-troposphere exchange).

The simulation with the $\Delta'(^{17}O)$ adjusted production term is in much better agreement than the original Lutjewad simulation, as can be seen in figure 7. It is striking that over the years 2019-2021 the model simulation follows the running average of the measurements very well with a correlation coefficient of 0.82 for this period. For the years 2017 and 2018 the data and the model agree in that there is much less interannual variability in both the measurements and the model simulation. However on the small scale variability the comparison is hampered by the relatively high uncertainty of the measurements. The overall variability over the full record is -0.19 to -0.07 ‰ for the model simulation and -0.27 to -0.16 ‰ for the moving average of the measurements. Although the absolute values of the measurements and the model differ by 0.08 ‰, the overall variability of the simulation with the adjusted $\Delta'(^{17}O)$ production term increased significantly and is close to the overall variability of the measurements. The much improved agreement of the model simulation and the measured $\Delta'(^{17}O)$ indicates the need for revising the stratospheric source of the model, now done using the empirical relation with stratospheric N_2O amount fractions. This will lead to a more realistic input of high $\Delta(^{17}O\text{-}CO_2)$ into the troposphere.

The added source production term linked to lower stratosphere temperature is chosen for the adjusted model simulation because of its connection to troposphere-stratosphere transport at higher latitudes, as well as its relation to ozone concentrations in the stratosphere. A weak polar vortex is accompanied by elevated stratospheric temperatures and more stratosphere to troposphere downwelling, while low stratosphere temperatures lead to a more stable polar vortex and therefore less downward transport (Newman et al., 2001; Kidston et al., 2015). On top of that, we should consider the role of ozone amount fractions in the stratosphere on the formation of CO_2 with high $\Delta'(^{17}O)$ values. Formation of polar stratospheric clouds, accelerating the destruction of ozone, is known to occur during anomalous cold conditions, when the polar vortex is strong and stable (Lawrence et al., 2020). We hypothesize that colder lower stratosphere temperatures at 60-90° N lead to enhanced ozone destruction in the polar vortex which in return might reduce the production of high $\Delta(^{17}O\text{-}CO_2)$ in the stratosphere during late winter and early spring in the Northern-Hemisphere (given the role of ozone in the production of $\Delta'(^{17}O)$ stratospheric CO_2, Yung et al.). This will result in generally lower $\Delta'(^{17}O)$ values in tropospheric CO_2 after that period. This ozone-dependent process would than add up to the atmospheric transport process to reduce the $\Delta'(^{17}O)$ budget in the troposphere. The considerations above indicate that especially in more anomalous stratospheric conditions, both at higher and lower than average temperatures, the stratospheric $\Delta'(^{17}O)$ source is likely to deviate from the linear fit of stratospheric N_2O amount fractions and $\Delta'(^{17}O)$ values in CO_2 as was used in Koren et al. (2019). We acknowledge that our empirical modification still does not accurately describe the intricate complexities of the stratospheric production of $\Delta'(^{17}O)$, but at least allows us to assess the relevance of the stratospheric source for the model simulation and points in a direction where further model improvements can be beneficial.

Summarizing, we do observe interannual changes in both the Lutjewad and Mace Head records, possibly caused by variations in the stratospheric source of enriched $\Delta'(^{17}O)$. No seasonal cycle, which would be an expected effect of the biosphere, is observed but stratosphere-troposphere exchange seems to cause the highest variations in $\Delta'(^{17}O)$.

4 Conclusion and outlook

In this study we showed that $\Delta'(^{17}O)$ measurements of atmospheric CO_2, as well as $\delta(^{13}C)$ and $\delta(^{18}O)$ measurements, can be performed using laser absorption spectroscopy, thereby drastically reducing sample preparation time in comparison with IRMS measurements. This opens the opportunity to do long-term monitoring studies or field studies more easily and can lead to an increase in $\Delta'(^{17}O)$ measurements of atmospheric CO_2 in the near future. With our analysis method we reach combined uncertainties of 0.05 ‰ when the sample CO_2 amount fraction is within the range of the reference gases, and the sample does not differ more than 15 µmol/mol from the nearest reference. Extrapolation of the calibration curves, or high differences between the sample and the nearest reference introduce uncertainty of the results, showing the importance of including enough reference gases in the calibration. For $\delta(^{13}C)$ and $\delta(^{18}O)$ measurements we reach combined uncertainties of 0.03 and 0.05 ‰ respectively, under good calibration conditions. Seasonal cycles, as well as long-term trends as can be expected from the known sources and sinks of ^{13}C and ^{18}O were clearly identified from the Lutjewad and Mace Head measurement records. The $\Delta'(^{17}O)$ records show significant interannual variability at both measurement locations. A seasonal cycle is not observed, possibly due to too high uncertainties of the measurement results. The measurement instrument will be used for semi-continuous measurements at the Lutjewad station in the near-future, resulting in much higher sampling frequency so rigorous filtering can be applied on the measurement results. In this way we hope to link variations in the records to specific events which will help us understand the $\Delta'(^{17}O)$ budget of atmospheric CO_2 in the troposphere better.

As original model simulations do not capture the interannual variability as observed in the measurements, we revised the model definition of stratospheric input of CO_2 with a high $\Delta'(^{17}O)$ value into the troposphere by linking it to temperature anomalies of the 60-90° N lowermost stratosphere as a proxy for the downwelling strength. This resulted in a much stronger interannual variability in the model simulation for the Lutjewad location, following the variations in $\Delta'(^{17}O)$ measurements closely for the years 2019-2021. This suggests that the interannual variability in the tropospheric budget of $\Delta'(^{17}O)$ as observed in the Lutjewad measurements is more strongly coupled to year-to-year variations in stratospheric downwelling of enhanced $\Delta'(^{17}O)$ values in CO_2 than previously assumed. ~~Our results show that the biosphere is not the dominant process for variations in $\Delta'(^{17}O)$. $\Delta'(^{17}O)$ of atmospheric CO_2 is therefore not suitable as a proxy for quantification for gross primary production at our study locations. The variation in the stratospheric source of high $\Delta'(^{17}O)$ is possibly the cause for the high interannual variations we observe in the records. We should therefore consider the potential of using $\Delta'(^{17}O)$ of atmospheric CO_2 as a proxy for stratospheric intrusion instead.~~

Data availability. Data presented in this paper can be downloaded from https://doi.org/10.34894/1XJG1F

Appendix A: $\delta(^{18}O)$ differences SICAS and IMAU flask measurements

$\delta(^{18}O)$ measurements of samples that should be identical conducted at the IMAU and with the SICAS differ strongly, as can be seen in figure A1. We argue that this is due to drift of the oxygen isotopes in the flasks, a phenomenon described in (Steur

et al., 2023). In figure A2 the difference in $\delta(^{18}O)$ (SICAS-IMAU) is plotted against the difference in storage time, for the flasks of which the date of CO_2 extraction is known. Especially the samples of which the CO_2 was extracted at the IMAU
485 show a negative trend, as expected from the fact that over time $\delta(^{18}O)$ values drift towards more negative values. The samples extracted at the CIO do not show this trend, possibly due to the fact that another extraction method was used, adding more uncertainty to the $\delta(^{18}O)$ values. The time that passed before samples were measured at the IMAU after extraction at the CIO is very variable. It is possible that the pure CO_2 samples drifted over time. This extra uncertainty factor is not included in this analysis.
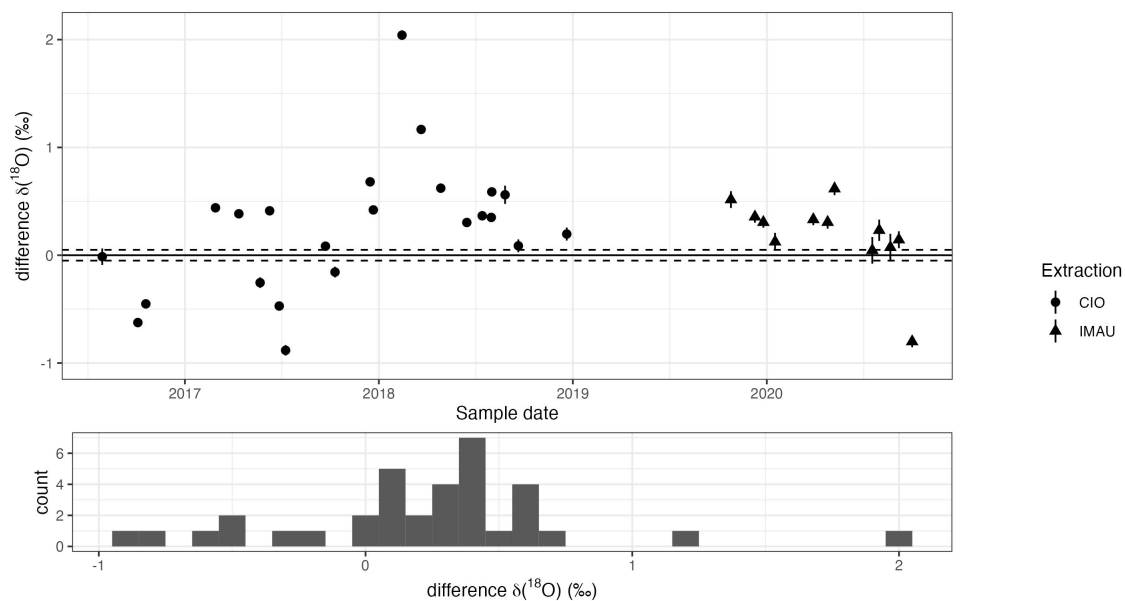
Figure A1. The top panel shows the differences (CIO-IMAU) of $\delta(^{18}O)$ measurements of the duplicate flasks. Uncertainty bars show the combined uncertainty of the CIO measurements. Shape of the data points indicates whether CO_2 was extracted at CIO and send to IMAU as pure CO_2 samples (circles) or whether extraction was done at IMAU (triangles). The lower panels shows the frequency distribution of the differences.
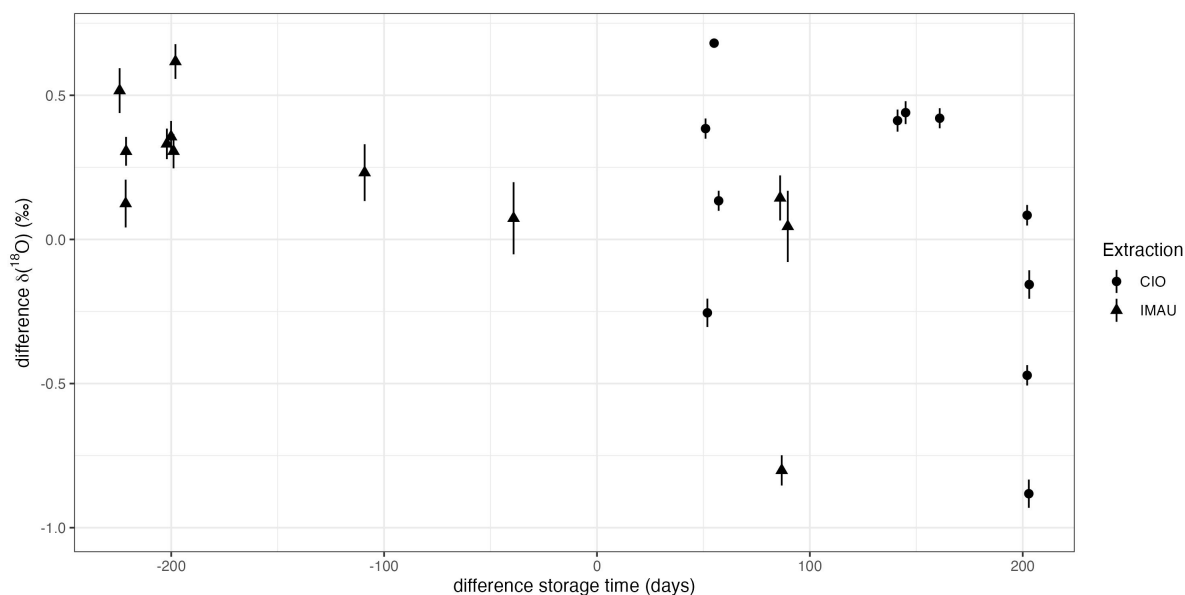
Figure A2. The differences of $\delta(^{18}O)$ measurements (CIO-IMAU) of the duplicate flasks is plotted against the difference in storage time (CIO-IMAU). Uncertainty bars show the combined uncertainty (+/- 1-σ) of the CIO measurements. The shape of the datapoints indicates whether samples were extracted at the CIO (circles) or at the IMAU (~~traingles~~triangles).

Appendix B: Sensitivity analysis drift of $\Delta'(^{17}O)$ in glass sample flasks

To determine the change in $\Delta'(^{17}O)$ as the result of drift of the oxygen isotopes of atmospheric CO_2 inside glass sample flasks (Steur et al., 2023), a simulation of the various changes was conducted. In an earlier study we showed that small amounts of water inside the flasks will change the original oxygen isotope composition of the atmospheric CO_2, as CO_2 and water will equilibrate. Water builds up inside the flasks over time, both through sampling and through permeation of water into the flask through the Viton O-rings (Steur et al., 2023). For the simulation we use flasks of 2.3 L containing air with a CO_2 amount fraction of 400 μmol/mol at atmospheric pressure. The initial $\delta(^{18}O)$ of the atmospheric CO_2 is 37 ‰ on the VSMOW scale, within the atmospheric range. The $\delta(^{17}O)$ varies such that there are simulations for initial $\Delta'(^{17}O)$ values of 0.31, -0.09, -0.19, -0.29, -0.69 ‰. These values were chosen as they correspond to variations around the water-CO_2 equilibration line with a λ of 0.5229 (Barkan and Luz, 2012). For the initial $\delta(^{18}O)$ and $\delta(^{17}O)$ of the water we use -12.91 and -6.77 ‰ VSMOW, respectively. The $\Delta'(^{17}O)$ value of the water is 0.07 ‰. These values are measurement results of extracted water from lab air, measured with a LGR OA-ICOS Liquid Water Isotope Analyzer. We assume that all CO_2 and water equilibrate over time. The amount of water inside the flask varies between 10^{-4} and 10^{-6} g, such that equilibration causes changes in $\delta(^{18}O)$ of the atmospheric CO_2 between -3.27 and -0.03 ‰. It should be noted that changes of more than 3 ‰ in $\delta(^{18}O)$ are very high, as changes of 0.48 ‰ were observed after 114 days of storage in similar conditions as described above (Steur et al., 2023). The

505 change in $\Delta'(^{17}O)$ of the atmospheric CO_2 ranges between -0.005 and 0.06 ‰ for all scenarios described above and is limited to -0.002 and 0.01 ‰ for a realistic maximum drift of -0.48 ‰ (see also figure B1).
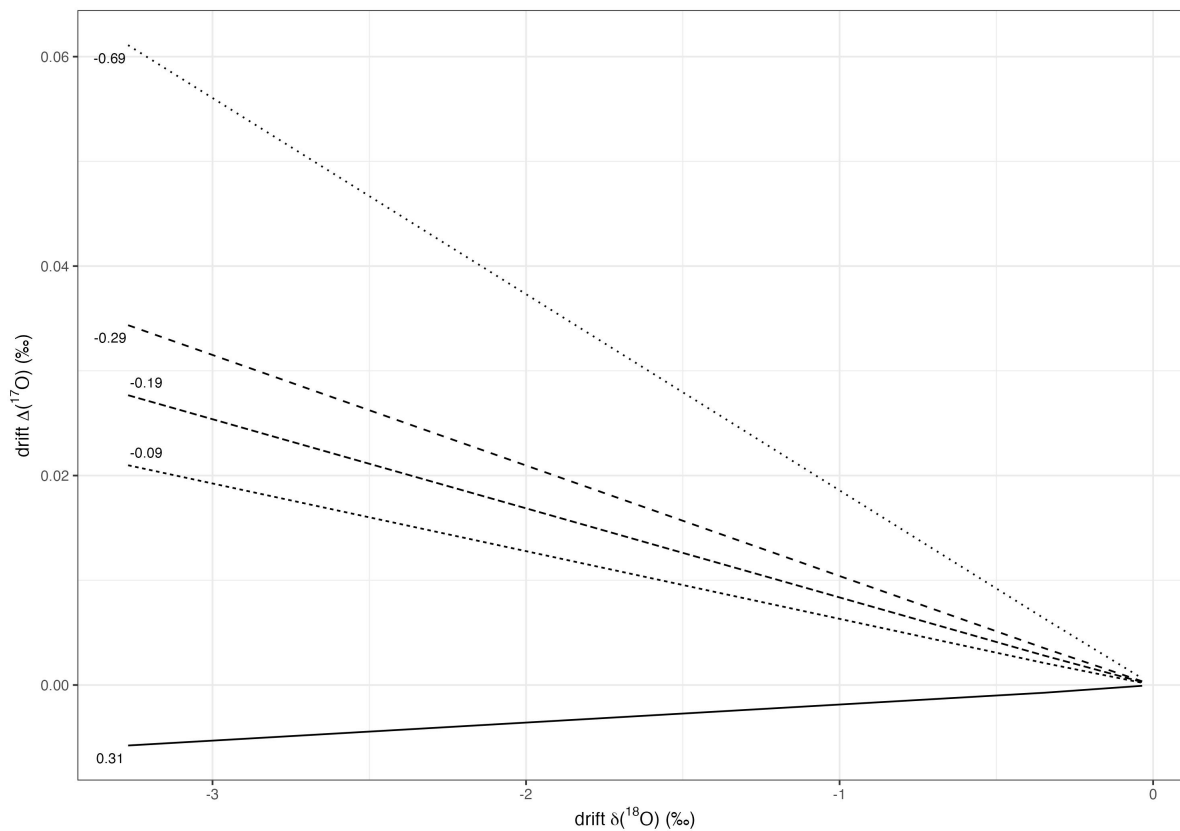
Figure B1. Results of a sensitivity analysis of the drift of $\Delta'(^{17}O)$ of atmospheric CO_2 in a 2.3 L glass sample flask as a function of the drift in $\delta(^{18}O)$. The initial $\Delta'(^{17}O)$ value of the atmospheric CO_2 is indicated per line.

Appendix C: Lutjewad $\Delta'(^{17}O)$ measurements from CIO and IMAU compared

Two identical flask samples (duplicates) have occasionally been taken at Lutjewad, with the aim to compare measurements of the SICAS with IRMS measurements from IMAU. For $\Delta'(^{17}O)$ measurements this comparison is hard to make, considering 510 the very low variance that is observed in the duplicate samples from the Lutjewad station. Also, not all duplicates have been measured by both labs. Figure C1 shows results of identical samples measured at IMAU and CIO in a space representative for the total range in $\Delta'(^{17}O)$ that was measured at Lutjewad. From the figure it is clear that the identical samples that were measured are not representing the full range of $\Delta'(^{17}O)$, ranging from -0.4 to -0.1 ‰. We should also consider the (undefined) uncertainty added by the extraction of the CO_2 from air, which is done for the IMAU measurements, but not for the SICAS 515 measurements.

When considering, however, all datapoints of the Lutjewad flasks from the SICAS and from the IMAU, significant interannual variability is reflected in both datasets. Both the IMAU and the SICAS measurements show lower values in 2020 than in the period before, as observed in figure C2.
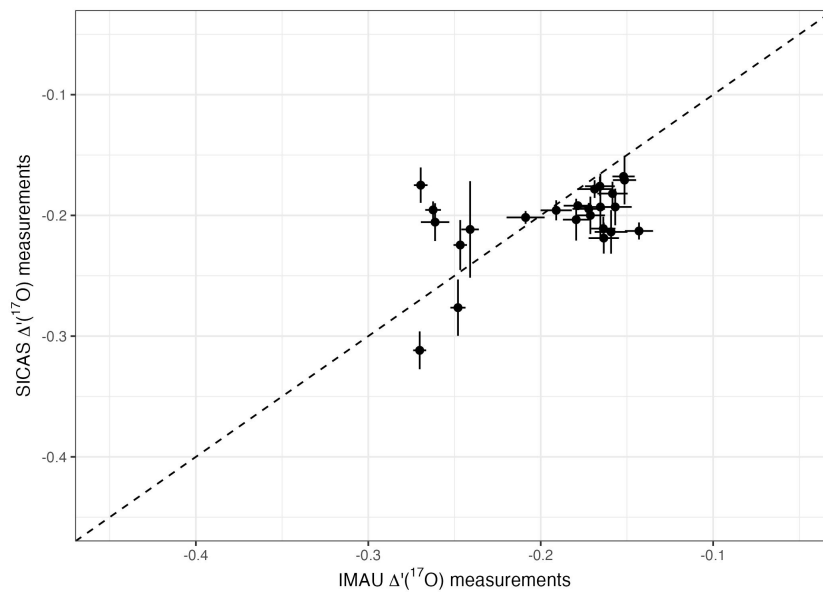
Figure C1. $\Delta'(^{17}O)$ measurements conducted with IRMS at IMAU (x-axis) and conducted with the SICAS (y-axis), all in ‰. The error bars show the standard errors of the measurements. The dashed line is the 1:1 ratio.
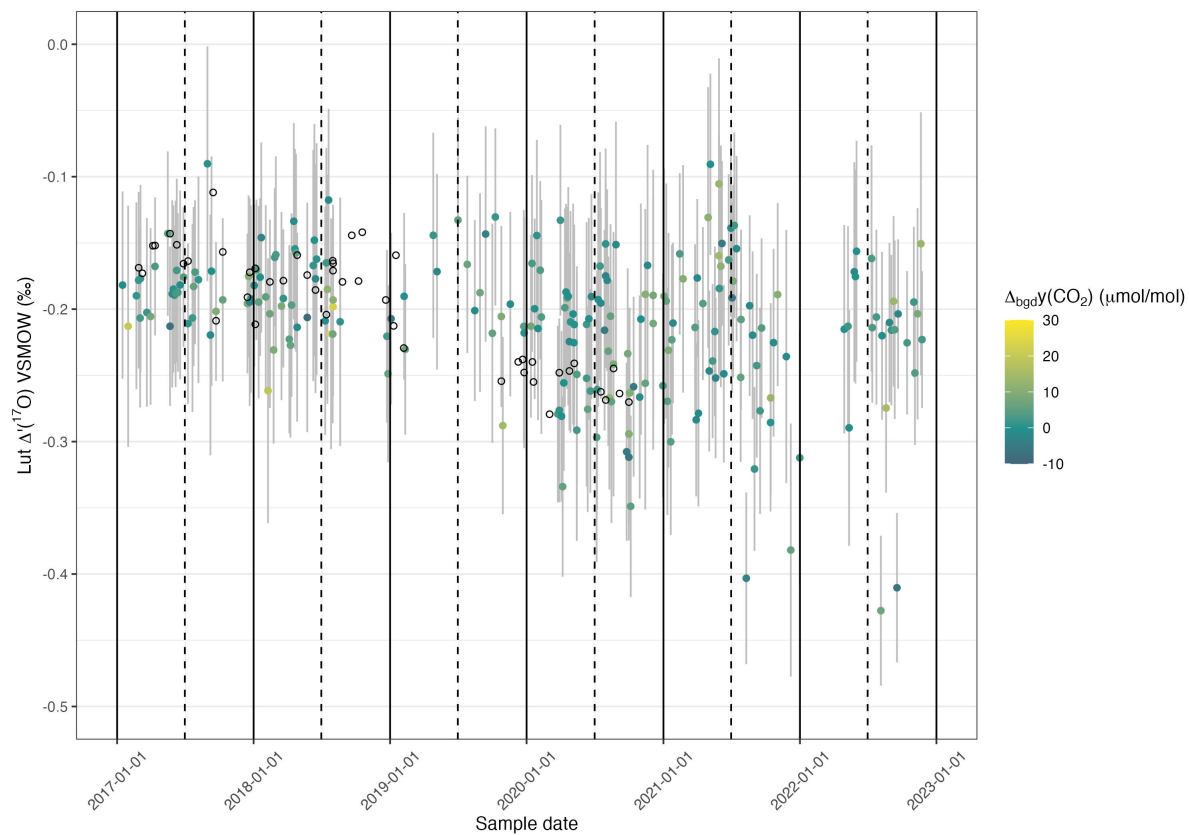
Figure C2. $\Delta^2(^{17}O)$ record of Lutjewad from SICAS flask measurements (filled circles) and DI-IRMS flask measurements of duplicate flasks from the IMAU (open circles). The combined uncertainties of the SICAS measurements are shown as the grey error bars (+/- 1-σ) and include measurement uncertainty, repeatability and accuracy and introduced uncertainty as a consequence of the calibration method used. The difference in amount fraction between the sample and the background curve, or ΔCO_2, is indicated by the colour of the data points.

Appendix D: Lutjewad $\Delta^2(^{17}O)$ seasonality plots
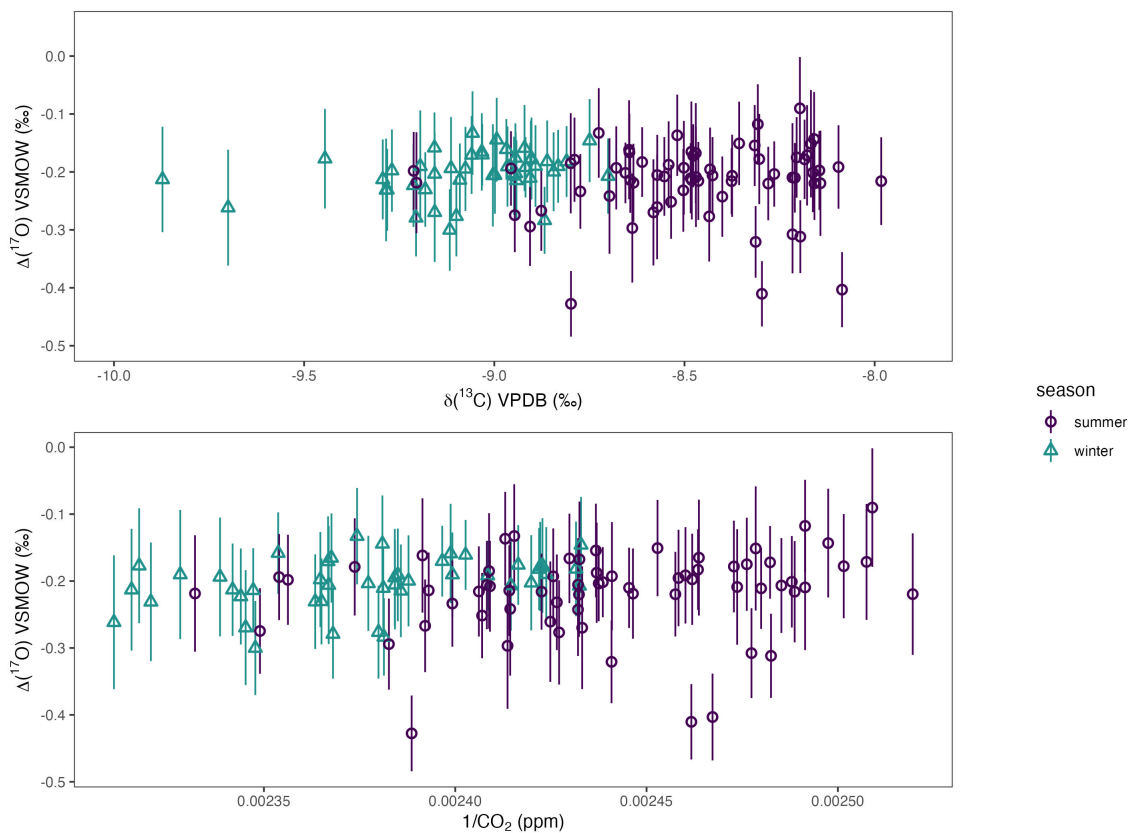
Figure D1. $\Delta^2(^{17}O)$ summer (July, August and September) and winter (January, February and March) values of Lutjewad plotted against $\delta(^{13}C)$ (upper) and $1/CO_2$ (lower). The uncertainty bars show the combined uncertainty (+/- 1-σ) of the $\Delta^2(^{17}O)$ SICAS measurements.

Appendix E: Estimation $\Delta^2(^{17}O)$ depletion due to equilibration with of CO_2 and plant water

In this analysis we make an estimate of the potential change in $\Delta^2(^{17}O)$ as the result of the equilibration of atmospheric CO_2 and plant water. The $\delta(^{18}O)$ value of atmospheric CO_2 is the result of multiple processes, but for simplicity we assume that the value is fully the result of the equilibration of CO_2 and plant water. The highest $\delta(^{18}O)$ for CO_2 measured in the Lutjewad record is 42.48 ‰ (VSMOW). To derive a value of 42.48 ‰, assuming the fractionation factor of 1.0412 for CO_2-H_2O equilibration, the leaf water will have a $\delta(^{18}O)$ of 1.23 ‰. Soil water in the Netherlands typically has a $\delta(^{18}O)$ of -7.5 ‰ (VSMOW) (Mook, 1970). We assume that the change in $\delta(^{18}O)$ between the soil water and the plant water is caused by evapotranspiration (fractionation factor is 0.9917 (West et al., 2008)) where the ~~Θ~~ θ is 0.516, the lowest value that was found by Landais et al. (2006). This will result in plant water with a $\delta(^{17}O)$ of 0.56 ‰ and a $\Delta^2(^{17}O)$ of -0.1 ‰. This $\Delta^2(^{17}O)$ value will translate to the CO_2 that equilibrates with the water.

Author contributions. WP and HM initiated and enabled the research. PS and HS conducted the spectral measurements. GA conducted the IRMS measurements. PS did the data analysis. GK performed the model simulations. PS wrote the text, HS and GK gave input for the discussion. All authors helped to finalise the manuscript.

Competing interests. The authors declare that they have no conflict of interest.

Acknowledgements. We thank Gerard Spain from the University of Galway for sampling of the Mace Head flasks for many years. Stable isotope composition measurements of the SICAS calibration gases were conducted at the Max Plank Institute for Biogeochemistry in Jena, and we thank Heiko Moossen and his team for that. The simulations were performed on the HPC cluster Aether at the University of Bremen, financed by DFG within the scope of the Excellence Initiative. This project has received funding from the EMPIR programme co-financed by the Participating States and from the European Union's Horizon 2020 research and innovation programme. WP, GA, and GK acknowledge funding from the European Research Council, for the ASICA project under grant (649087). Finally, we thank the editor Jan Kaiser and the two anonymous reviewers for taking the time and effort to provide us with comments and suggestions to improve the manuscript.

References

Adnew, G. A., Hofmann, M. E. G., Paul, D., Laskar, A., Surma, J., Albrecht, N., Pack, A., Schwieters, J., Koren, G., Peters, W., and Röckmann, T.: Determination of the triple oxygen and carbon isotopic composition of CO_2 from atomic ion fragments formed in the ion source of the 253 Ultra high-resolution isotope ratio mass spectrometer, Rapid Communications in Mass Spectrometry, 33, 1363–1380, https://doi.org/10.1002/rcm.8478, 2019.

Adnew, G. A., Pons, T. L., Koren, G., Peters, W., and Röckmann, T.: Leaf-scale quantification of the effect of photosynthetic gas exchange on $\delta^{17}O$ of atmospheric CO_2, Biogeosciences, 17, 3903–3922, https://doi.org/10.5194/bg-17-3903-2020, 2020.

Adnew, G. A., Workman, E., Janssen, C., and Röckmann, T.: Temperature dependence of isotopic fractionation in the CO2-O2 isotope exchange reaction, Rapid Communications in Mass Spectrometry, 36, e9301, 2022.

Adnew, G. A., Pons, T. L., Koren, G., Peters, W., and Röckmann, T.: Exploring the potential of $\Delta^{17}O$ in CO_2 for determining mesophyll conductance, Plant Physiology, 192, 1234–1253, https://doi.org/10.1093/plphys/kiad173, 2023.

Assonov, S. S., Brenninkmeijer, C. A. M., Schuck, T. J., and Taylor, P.: Analysis of ^{13}C and ^{18}O isotope data of CO_2 in CARIBIC aircraft samples as tracers of upper troposphere/lower stratosphere mixing and the global carbon cycle, Atmospheric Chemistry and Physics, 10, 8575–8599, https://doi.org/10.5194/acp-10-8575-2010, 2010.

Bajnai, D., Pack, A., Arduin Rode, F., Seefeld, M., Surma, J., and Di Rocco, T.: A Dual Inlet System for Laser Spectroscopy of Triple Oxygen Isotopes in Carbonate-Derived and Air CO2, Geochemistry, Geophysics, Geosystems, 24, e2023GC010 976, 2023.

Barkan, E. and Luz, B.: High-precision measurements of $^{17}O/^{16}O$ and $^{18}O/^{16}O$ ratios in CO_2, Rapid Communications in Mass Spectrometry, 26, 2733–2738, https://doi.org/10.1002/rcm.6400, 2012.

Boering, K. A., Jackson, T., Hoag, K. J., Cole, A. S., Perri, M. J., Thiemens, M., and Atlas, E.: Observations of the anomalous oxygen isotopic composition of carbon dioxide in the lower stratosphere and the flux of the anomaly to the troposphere, Geophysical Research Letters, 31, 1–5, https://doi.org/10.1029/2003GL018451, 2004.

Bânddă, N., Krol, M., van Noije, T., van Weele, M., Williams, J. E., Sager, P. L., Niemeier, U., Thomason, L., and Röckmann, T.: The effect of stratospheric sulfur from Mount Pinatubo on tropospheric oxidizing capacity and methane, Journal of Geophysical Research: Atmospheres, 120, 1202–1220, https://doi.org/https://doi.org/10.1002/2014JD022137, 2015.

Carlstad, J. M. and Boering, K. A.: Isotope effects and the atmosphere, Annual Review of Physical Chemistry, 74, 439–465, 2023.

Chen, H., Winderlich, J., Gerbig, C., Katrynski, K., Jordan, A., and Heimann, M.: Validation of routine continuous airborne CO_2 observations near the Bialystok Tall Tower, Atmospheric Measurement Techniques, 5, 873–889, https://doi.org/10.5194/amt-5-873-2012, 2012.

Ciais, P., Tans, P. P., Trolier, M., White, J. W. C., and Francey, R. J.: A large Northern Hemisphere terrestrial CO_2 sink indicated by the $^{13}C/^{12}C$ ratio of atmospheric CO_2, Science, 269, 1098–1102, 1995.

Ciais, P., Denning, A. S., Tans, P. P., Berry, J. A., Randall, D. A., Collatz, G. J., Sellers, P. J., White, J. W. C., Trolier, M., Meijer, H. A. J., Francey, R. J., Monfray, P., and Heimann, M.: A three-dimensional synthesis study of ^{18}O in atmospheric CO_2 1. Surface fluxes, Journal of Geophysical Research Atmospheres, 102, 5857–5872, https://doi.org/10.1029/96jd02360, 1997.

Dee, D. P., Uppala, S. M., Simmons, A. J., Berrisford, P., Poli, P., Kobayashi, S., Andrae, U., Balmaseda, M. A., Balsamo, G., Bauer, P., Bechtold, P., Beljaars, A. C. M., van de Berg, L., Bidlot, J., Bormann, N., Delsol, C., Dragani, R., Fuentes, M., Geer, A. J., Haimberger, L., Healy, S. B., Hersbach, H., Hólm, E. V., Isaksen, L., Kållberg, P., Köhler, M., Matricardi, M., McNally, A. P., Monge-Sanz, B. M., Morcrette, J.-J., Park, B.-K., Peubey, C., de Rosnay, P., Tavolato, C., Thépaut, J.-N., and Vitart, F.: The ERA-Interim reanalysis:

configuration and performance of the data assimilation system, Quarterly Journal of the Royal Meteorological Society, 137, 553–597, https://doi.org/10.1002/qj.828, 2011.

Francey, R. J. and Tans, P. P.: Latitudinal variation in oxygen-18 of atmospheric CO2, Nature, 327, 495–497, 1987.

580 Friedlingstein, P., Jones, M. W., O'sullivan, M., Andrew, R. M., Bakker, D. C., Hauck, J., Le Quéré, C., Peters, G. P., Peters, W., Pongratz, J., et al.: Global carbon budget 2021, Earth System Science Data, 14, 1917–2005, 2022.

Griffith, D. W., Deutscher, N. M., Caldow, C., Kettlewell, G., Riggenbach, M., and Hammer, S.: A Fourier transform infrared trace gas and isotope analyser for atmospheric applications, Atmospheric Measurement Techniques, 5, 2481–2498, https://doi.org/10.5194/amt-5-2481-2012, 2012.

585 Hare, V. J., Dyroff, C., Nelson, D. D., and Yarian, D. A.: High-Precision Triple Oxygen Isotope Analysis of Carbon Dioxide by Tunable Infrared Laser Absorption Spectroscopy, Analytical Chemistry, https://doi.org/10.1021/acs.analchem.2c03005, 2022.

Hersbach, H., Bell, B., Berrisford, P., Hirahara, S., Horányi, A., Muñoz-Sabater, J., Nicolas, J., Peubey, C., Radu, R., Schepers, D., Simmons, A., Soci, C., Abdalla, S., Abellan, X., Balsamo, G., Bechtold, P., Biavati, G., Bidlot, J., Bonavita, M., De Chiara, G., Dahlgren, P., Dee, D., Diamantakis, M., Dragani, R., Flemming, J., Forbes, R., Fuentes, M., Geer, A., Haimberger, L., Healy, S., Hogan, R. J.,

590 Hólm, E., Janisková, M., Keeley, S., Laloyaux, P., Lopez, P., Lupu, C., Radnoti, G., de Rosnay, P., Rozum, I., Vamborg, F., Villaume, S., and Thépaut, J.-N.: The ERA5 global reanalysis, Quarterly Journal of the Royal Meteorological Society, 146, 1999–2049, https://doi.org/https://doi.org/10.1002/qj.3803, 2020.

Hillaire-Marcel, C., Kim, S.-T., Landais, A., Ghosh, P., Assonov, S., Lécuyer, C., Blanchard, M., Meijer, H. A. J., and Steen-Larsen, H. C.: A stable isotope toolbox for water and inorganic carbon cycle studies, Nature Reviews Earth Environment, 2, 699–719,

595 https://doi.org/10.1038/s43017-021-00209-0, 2021.

Hoag, K. J., Still, C. J., Fung, I. Y., and Boering, K. A.: Triple oxygen isotope composition of tropospheric carbon dioxide as a tracer of terrestrial gross carbon fluxes, Geophysical Research Letters, 32, 1–5, https://doi.org/10.1029/2004GL021011, 2005.

Hofmann, M. E. G., Horváth, B., Schneider, L., Peters, W., Schützenmeister, K., and Pack, A.: Atmospheric measurements of $\Delta^{17}O$ in CO_2 in Göttingen, Germany reveal a seasonal cycle driven by biospheric uptake, Geochimica et Cosmochimica Acta,

600 https://doi.org/10.1016/j.gca.2016.11.019, 2017.

Horváth, B., Hofmann, M. E., and Pack, A.: On the triple oxygen isotope composition of carbon dioxide from some combustion processes, Geochimica et Cosmochimica Acta, 95, 160–168, https://doi.org/10.1016/j.gca.2012.07.021, 2012.

Kaiser, J., Forster, G., Pickers, P., A., M., A., M., and L., F.: Polyisotopic carbon dioxide ratios at the coastal Weybourne Atmospheric Observatory (Norfolk, UK), 12th International Symposium on Isotopomers, 12th Isotope Conference, Dübendorf, Switzerland, 2022.

605 Kawagucci, S., Tsunogai, U., Kudo, S., Nakagawa, F., Honda, H., Aoki, S., Nakazawa, T., Tsutsumi, M., and Gamo, T.: Long-term observation of mass-independent oxygen isotope anomaly in stratospheric CO2, Atmospheric Chemistry and Physics, 8, 6189–6197, https://doi.org/10.5194/acp-8-6189-2008, 2008.

Keeling, C. D.: The Suess effect: [13]Carbon-[14]Carbon interrelations, Environment International, 2, 229–300, 1979.

Keeling, C. D., Carter, A. F., and Mook, W. G.: Seasonal, latitudinal, and secular variations in the abundance and isotopic ratios of atmo-

610 spheric CO2 2. Results from oceanographic cruises in the Tropical Pacific Ocean., Journal of Geophysical Research, 89, 4615–4628, https://doi.org/10.1029/JD089iD03p04615, 1984.

Keeling, C. D., Piper, . C., Bacastow, R. B., Wahlen, ., Whorf, T. P., Heimann, M., and Meijer, H. A. J.: Atmospheric CO_2 and $^{13}CO_2$ exchange with the terrestrial biosphere and oceans from 1978 to 2000: Observations and carbon cycle implications, pp. 83–113, Springer-Verlag, https://doi.org/10.1007/0-387-27048-5_5, 2005.

615   Keeling, R. F., Graven, H. D., Welp, L. R., Resplandy, L., Bi, J., Piper, S. C., Sun, Y., Bollenbacher, A., and Meijer, H. A. J.: Atmospheric evidence for a global secular increase in carbon isotopic discrimination of land photosynthesis, Proceedings of the National Academy of Sciences of the United States of America, 114, 10 361–10 366, https://doi.org/10.1073/pnas.1619240114, 2017.

Kidston, J., Scaife, A. A., Hardiman, S. C., Mitchell, D. M., Butchart, N., Baldwin, M. P., and Gray, L. J.: Stratospheric influence on tropospheric jet streams, storm tracks and surface weather, Nature Geoscience, 8, 433–440, 2015.

620   Koren, G., Schneider, L., van der Velde, I. R., van Schaik, E., Gromov, S. S., Adnew, G. A., Martino, D. J. M., Hofmann, M. E. G., Liang, M.-C., Mahata, S., Bergamaschi, P., van der Laan-Luijkx, I. T., Krol, M. C., Röckmann, T., and Peters, W.: Global 3-D simulations of the triple oxygen isotope signature $\Delta^{17}O$ in atmospheric CO_2, Journal of Geophysical Research: Atmospheres, 124, 8808–8836, https://doi.org/10.1029/2019jd030387, 2019.

Laan, S. V. D., Neubert, R. E. M., and Meijer, H. A. J.: A single gas chromatograph for accurate atmospheric mixing ratio measurements of

625   CO_2, CH_4, N_2O, SF_6 and CO, Atmospheric Measurement Techniques, 2, 549–559, www.atmos-meas-tech.net/2/549/2009/, 2009.

Lan, X., Dlugokencky, E., Mund, J., Crotwell, A. M., Crotwell, M., Moglia, E., Madronich, M., Neff, D., and Thoning, K. W.: Atmospheric carbon dioxide dry air mole fractions from the NOAA GML carbon cycle cooperative global air sampling network, 1968-2021, 2022.

Landais, A., Barkan, E., Yakir, D., and Luz, B.: The triple isotopic composition of oxygen in leaf water, Geochimica et Cosmochimica Acta, 70, 4105–4115, https://doi.org/10.1016/j.gca.2006.06.1545, 2006.

630   Laskar, A. H., Mahata, S., and Liang, M. C.: Identification of anthropogenic CO_2 using triple oxygen and clumped isotopes, Environmental Science and Technology, 50, 11 806–11 814, https://doi.org/10.1021/acs.est.6b02989, 2016.

Lawrence, Z. D., Perlwitz, J., Butler, A. H., Manney, G. L., Newman, P. A., Lee, S. H., and Nash, E. R.: The Remarkably Strong Arctic Stratospheric Polar Vortex of Winter 2020: Links to Record-Breaking Arctic Oscillation and Ozone Loss, Journal of Geophysical Research: Atmospheres, 125, https://doi.org/10.1029/2020JD033271, 2020.

635   Levin, I., Ciais, P., Langenfelds, R., Schmidt, M., Ramonet, M., Sidorov, K., Tchebakova, N., Gloor, M., Heimann, M., Schulze, E.-D., Vygodskaya, N. N., Shibistova, O., and Lloyd, J.: Three years of trace gas observations over the EuroSiberian domain derived from aircraft sampling — a concerted action, Tellus B: Chemical and Physical Meteorology, 54, 696–712, https://doi.org/10.3402/tellusb.v54i5.16717, 2002.

Liang, M. C. and Mahata, S.: Oxygen anomaly in near surface carbon dioxide reveals deep stratospheric intrusion, Scientific Reports, 5,

640   https://doi.org/10.1038/srep11352, 2015.

Liang, M. C., Mahata, S., Laskar, A. H., and Bhattacharya, S. K.: Spatiotemporal variability of oxygen isotope anomaly in near surface air CO_2 over urban, semi-urban and ocean areas in and around Taiwan, Aerosol and Air Quality Research, 17, 706–720, https://doi.org/10.4209/aaqr.2016.04.0171, 2017.

Liang, M.-C., Laskar, A. H., Barkan, E., Newman, S., Thiemens, M. H., and Rangarajan, R.: New constraints of terrestrial and oceanic global

645   gross primary productions from the triple oxygen isotopic composition of atmospheric CO2 and O2, Scientific reports, 13, 2162, 2023.

Lämmerzahl, P., Röckmann, T., Brenninkmeijer, C. A. M., Krankowsky, D., and Mauersberger, K.: Oxygen isotope composition of stratospheric carbon dioxide, Geophysical Research Letters, 29, 23–1–23–4, https://doi.org/10.1029/2001GL014343, 2002.

Mahata, S., Bhattacharya, S. K., Wang, C. H., and Liang, M. C.: Oxygen isotope exchange between O2 and CO2 over hot platinum: An innovative technique for measuring Δ17O in CO 2, Analytical Chemistry, 85, 6894–6901, https://doi.org/10.1021/ac4011777, 2013.

650   Meijer, H. A. J. and Li, W. J.: The use of electrolysis for accurate $\delta^{17}O$ and $\delta^{18}O$ isotope measurements in water, Isotopes in Environmental and Health Studies, 34, 349–369, https://doi.org/10.1080/10256019808234072, 1998.

Miller, M. F. and Pack, A.: Why Measure 17O? Historical perspective, triple-isotope systematics and selected applications, https://doi.org/10.2138/rmg.2021.86.01, 2021.

Mook, W.: Stable carbon and oxygen isotopes of natural waters in the Netherlands, Isotope hydrology, 1970, 163–190, 1970.

655 Mook, W. G., Koopmans, M., Carter, A. F., and Keeling, C. D.: Seasonal, latitudinal, and secular variations in the abundance and isotopic ratios of atmospheric carbon dioxide (South Pole, Pacific Ocean). 1. Results from land stations., Journal of Geophysical Research, 88, 10 915–10 933, https://doi.org/10.1029/JC088iC15p10915, 1983.

Neubert, R. E. M., Spijkervet, L. L., Schut, J. K., Been, H. A., and Meijer, H. A.: A computer-controlled continuous air drying and flask sampling system, Journal of Atmospheric and Oceanic Technology, 21, 651–659, https://doi.org/10.1175/1520-

660 0426(2004)021<0651:ACCADA>2.0.CO;2, 2004.

Nevison, C. D., Mahowald, N. M., Weiss, R. F., and Prinn, R. G.: Interannual and seasonal variability in atmospheric N_2O, Global Biogeochemical Cycles, 21, https://doi.org/10.1029/2006GB002755, 2007.

Nevison, C. D., Dlugokencky, E., Dutton, G., Elkins, J. W., Fraser, P., Hall, B., Krummel, P. B., Langenfelds, R. L., Prinn, R. G., Steele, L. P., and Weiss, R. F.: Abiotic and biogeochemical signals derived from the seasonal cycles of tropospheric nitrous oxide, Atmos. Chem.

665 Phys. Discuss, 10, 25 803–25 839, https://doi.org/10.5194/acpd-10-25803-2010, 2010.

Newman, P. A., Nash, E. R., and Rosenfield, J. E.: What controls the temperature of the Arctic stratosphere during the spring?, Journal of Geophysical Research: Atmospheres, 106, 19 999–20 010, 2001.

Perdue, N., Sharp, Z., Nelson, D., Wehr, R., and Dyroff, C.: A rapid high-precision analytical method for triple oxygen isotope analysis of CO2 gas using tunable infrared laser direct absorption spectroscopy, Rapid Communications in Mass Spectrometry, 36,

670 https://doi.org/10.1002/rcm.9391, 2022.

Peters, W., van der Velde, I. R., van Schaik, E., Miller, J. B., Ciais, P., Duarte, H. F., van der Laan-Luijkx, I. T., van der Molen, M. K., Scholze, M., Schaefer, K., Vidale, P. L., Verhoef, A., Wårlind, D., Zhu, D., Tans, P. P., Vaughn, B., and White, J. W. C.: Increased water-use efficiency and reduced CO2 uptake by plants during droughts at a continental scale, Nature Geoscience, 11, 744–748, https://doi.org/10.1038/s41561-018-0212-7, 2018.

675 Peters, W., Bastos, A., Ciais, P., and Vermeulen, A.: A historical, geographical and ecological perspective on the 2018 European summer drought, Philosophical transactions of the Royal Society of London. Series B, Biological sciences, 375, 20190 505, https://doi.org/10.1098/rstb.2019.0505, 2020.

Ramonet, M., Ciais, P., Apadula, F., Bartyzel, J., Bastos, A., Bergamaschi, P., Blanc, P. E., Brunner, D., Torchiarolo, L. C. D., Calzolari, F., Chen, H., Chmura, L., Colomb, A., Conil, S., Cristofanelli, P., Cuevas, E., Curcoll, R., Delmotte, M., Sarra, A. D., Emmenegger, L.,

680 Forster, G., Frumau, A., Gerbig, C., Gheusi, F., Hammer, S., Haszpra, L., Hatakka, J., Hazan, L., Heliasz, M., Henne, S., Hensen, A., Hermansen, O., Keronen, P., Kivi, R., Komínková, K., Kubistin, D., Laurent, O., Laurila, T., Lavric, J. V., Lehner, I., Lehtinen, K. E., Leskinen, A., Leuenberger, M., Levin, I., Lindauer, M., Lopez, M., Myhre, C. L., Mammarella, I., Manca, G., Manning, A., Marek, M. V., Marklund, P., Martin, D., Meinhardt, F., Mihalopoulos, N., Mölder, M., Morgui, J. A., Necki, J., O'Doherty, S., O'Dowd, C., Ottosson, M., Philippon, C., Piacentino, S., Pichon, J. M., Plass-Duelmer, C., Resovsky, A., Rivier, L., Rodó, X., Sha, M. K., Scheeren, H. A., Sferlazzo,

685 D., Spain, T. G., Stanley, K. M., Steinbacher, M., Trisolino, P., Vermeulen, A., Vítková, G., Weyrauch, D., Xueref-Remy, I., Yala, K., and Kwok, C. Y.: The fingerprint of the summer 2018 drought in Europe on ground-based atmospheric CO_2 measurements: Atmospheric CO_2 anomaly, Philosophical Transactions of the Royal Society B: Biological Sciences, 375, https://doi.org/10.1098/rstb.2019.0513, 2020.

Rayner, P. J., Law, R. M., Allison, C. E., Francey, R. J., Trudinger, C. M., and Pickett-Heaps, C.: Interannual variability of the global carbon cycle (1992-2005) inferred by inversion of atmospheric CO_2 and $\delta^{13}CO_2$ measurements, Global Biogeochemical Cycles, 22, 1–12, https://doi.org/10.1029/2007GB003068, 2008.

Roeloffzen, J. C., Mook, W. G., and Keeling, C. D.: Trend and variations in stable carbon isotopes of atmospheric carbon dioxide, Stable isotopes in plant nutrition, soil fertility and environmental studies, pp. 601–618, 1991.

Scholze, M., Ciais, P., and Heimann, M.: Modelling terrestrial ^{13}C cycling: Climate, land use and fire, Global Biogeochemical Cycles, 22, https://doi.org/10.1029/2006GB002899, 2008.

Smith, N. E., Kooijmans, L. M. J., Koren, G., Schaik, E. V., Woude, A. M. V. D., Wanders, N., Ramonet, M., Xueref-Remy, I., Siebicke, L., Manca, G., Brümmer, C., Baker, I. T., Haynes, K. D., Luijkx, I. T., and Peters, W.: Spring enhancement and summer reduction in carbon uptake during the 2018 drought in northwestern Europe, Philosophical Transactions of the Royal Society B: Biological Sciences, 375, https://doi.org/10.1098/rstb.2019.0509, 2020.

Stanley, K. M., Grant, A., O'Doherty, S., Young, D., Manning, A. J., Stavert, A. R., Spain, T. G., Salameh, P. K., Harth, C. M., Simmonds, P. G., Sturges, W. T., Oram, D. E., and Derwent, R. G.: Greenhouse gas measurements from a UK network of tall towers: Technical description and first results, Atmospheric Measurement Techniques, 11, 1437–1458, https://doi.org/10.5194/amt-11-1437-2018, 2018.

Steur, P. M.: Using laser absorption spectroscopy for the measurement of $\delta^{13}C$, $\delta^{18}O$ and $\Delta^{17}O$ of atmospheric CO_2, Ph.D. thesis, University of Groningen, 2023.

Steur, P. M., Scheeren, H. A., Nelson, D. D., McManus, J. B., and Meijer, H. A. J.: Simultaneous measurement of $\delta^{13}C$, $\delta^{18}O$ and $\delta^{17}O$ of atmospheric CO_2- performance assessment of a dual-laser absorption spectrometer, Atmospheric Measurement Techniques, 14, 4279–4304, https://doi.org/10.5194/amt-14-4279-2021, 2021.

Steur, P. M., Botter, D., Scheeren, H. A., Moossen, H., Rothe, M., and Meijer, H. A.: Preventing drift of oxygen isotopes of CO_2-in-air stored in glass sample flasks: new insights and recommendations, Isotopes in Environmental and Health Studies, https://doi.org/10.1080/10256016.2023.2234594, 2023.

Stoltmann, T., Casado, M., Daëron, M., Landais, A., and Kassi, S.: Direct, precise measurements of isotopologue abundance ratios in CO_2 using molecular absorption spectroscopy: application to $\Delta^{17}O$, Analytical Chemistry, 89, 10 129–10 132, https://doi.org/10.1021/acs.analchem.7b02853, 2017.

Thiemens, M. H., Jackson, T. L., and Brenninkmeijer, C. A. M.: Observation of a mass independent oxygen isotopic composition in terrestrial stratospheric CO_2, the link to ozone chemistry, and the possible occurrence in the Martian atmosphere, Geophysical Research Letters, 22, 255–257, https://doi.org/10.1029/94GL02996, 1995.

Thiemens, M. H., Chakraborty, S., and Jackson, T. L.: Decadal $\Delta^{17}O$ record of tropospheric CO_2: Verification of a stratospheric component in the troposphere, Journal of Geophysical Research, 119, 6221–6229, https://doi.org/10.1002/2013JD020317, 2014.

van der Woude, A. M., Peters, W., Joetzjer, E., Lafont, S., Koren, G., Ciais, P., Ramonet, M., Xu, Y., Bastos, A., Botía, S., et al.: Temperature extremes of 2022 reduced carbon uptake by forests in Europe, nature communications, 14, 6218, 2023.

Welp, L. R., Keeling, R. F., Meijer, H. A. J., Bollenbacher, A. F., Piper, S. C., Yoshimura, K., Francey, R. J., Allison, C. E., and Wahlen, M.: Interannual variability in the oxygen isotopes of atmospheric CO2 driven by El Niño, Nature, 477, 579–582, https://doi.org/10.1038/nature10421, 2011.

Wendeberg, M., Richter, J. M., Rothe, M., and Brand, W. A.: Jena Reference Air Set (JRAS): A multi-point scale anchor for isotope measurements of CO_2 in air, Atmospheric Measurement Techniques, 6, 817–822, https://doi.org/10.5194/amt-6-817-2013, 2013.

West, J. B., Sobek, A., and Ehleringer, J. R.: A simplified GIS approach to modeling global leaf water isoscapes, PLoS one, 3, e2447, 2008.

Wiegel, A. A., Cole, A. S., Hoag, K. J., Atlas, E. L., Schauffler, S. M., and Boering, K. A.: Unexpected variations in the triple oxygen isotope composition of stratospheric carbon dioxide, Proceedings of the National Academy of Sciences, 110, 17680–17685, https://doi.org/10.1073/pnas.1213082110, 2013.

Wingate, L., Ogée, J., Cuntz, M., Genty, B., Reiter, I., Seibt, U., Yakir, D., Maseyk, K., Pendall, E. G., Barbour, M. M., et al.: The impact of soil microorganisms on the global budget of $\delta^{18}O$ in atmospheric CO_2, Proceedings of the National Academy of Sciences, 106, 22411–22415, 2009.

Worthy, D. E. J., Platt, A., Kessler, R., Ernst, M., Braga, R., and Racki, S.: The Canadian Atmospheric Carbon Dioxide Measurement Program: Measurement Procedures, Data Quality and Accuracy, Report of the 11th WMO/IAEA Meeting of Experts on Carbon Dioxide Concentration and Related Tracer Measurement Techniques, pp. 112–128, 2003.

Young, E. D., Galy, A., and Nagahara, H.: Kinetic and equilibrium mass-dependent isotope fractionation laws in nature and their geochemical and cosmochemical significance, Geochimica et Cosmochimica Acta, 66, 1095–1104, https://doi.org/10.1016/S0016-7037(01)00832-8, 2002.

Yung, Y. L., DeMore, W. B., and Pinto, J. P.: Isotopic exchange between carbon dioxide and ozone via O(^{1}D) in the stratosphere, Geophysical Research Letters, pp. 13–16.